Nongeostrophic Theory of Zonally Averaged Circulation. Part II: Eliassen–Palm Flux Divergence and Isentropic Mixing Coefficient

H. YANG, K. K. TUNG AND E. OLAGUER

Department of Applied Mathematics, University of Washington, Seattle, Washington

(Manuscript received 23 January 1989, in final form 23 August 1989)

ABSTRACT

We perform a diagnostic study of Eliassen–Palm flux divergence ($\Box \cdot F$), and isentropic mixing coefficient (K_{yy}) in the stratosphere for different seasons and for both hemispheres, taking into account nongeostrophic effects. An easily implementable procedure is given which yields a K_{yy} field that is consistent with advective transport. Evidence shows that the resultant time and space varying structure of K_{yy}, which is of the order of 10^5 m^2 s^{-1} in tropics and high latitudes but larger ($\sim 10^6$ m^2 s^{-1}) in the midlatitudes in the jet region, leads to improved simulation of stratospheric species whose distributions are affected by dynamical transport.

1. Introduction

Recent interest in the study of eddy Eliassen–Palm flux divergence reflects the general recognition that this quantity represents one of the main driving mechanisms of the zonal mean meridional circulation (Andrews and McIntyre 1978a,b; Andrews et al. 1983). Most existing results (Palmer and Hsu 1983; Hartmann et al. 1984; Geller et al. 1983, 1984; Clough et al. 1985) use a quasi-geostrophic form of the Eliassen–Palm flux divergence. In Part I (Tung 1986; and independently Andrews et al. 1987), a generalized Eliassen–Palm flux divergence is given, taking into account finite amplitude, nongeostrophic and diabatic effects. The present paper is concerned with a diagnostic study of this quantity in its more general form in different seasons in the stratosphere and for both the Northern and Southern hemispheres.

Another motivation for studying the Eliassen–Palm flux divergence is the central role that it plays in a self-consistent formulation of zonally averaged (the so-called 2-D) model of tracer transport. It is now known that in the lower stratosphere zonal mean transport mainly takes the form of advection by the mean diabatic circulation in the meridional plane and eddy mixing approximately along isentropic surfaces (Mahlman et al. 1984; Tung 1984). These two forms of transport are probably not independent (Mahlman et al. 1984; WMO 1986, chapter 6; Holton 1986; Newman et al. 1986; Plumb and Mahlman 1987). The mean diabatic heating, $\bar{Q}$, and the isentropic mixing coefficients, K_{yy}, can be related, in quasi-geostrophic theory, through the Eliassen–Palm flux divergence, making use of the crucial Taylor (1915) formula (Bretherton 1966; Dickinson 1969; Edmon et al. 1980). These relationships have been generalized in Part I in a nongeostrophic formulation in isentropic coordinates. It now appears that the theoretical foundations are nearly ready for us to perform a preliminary global diagnostic study of Eliassen–Palm flux divergence and isentropic mixing coefficients, and to assess the feasibility of incorporating the above-mentioned self-consistent constraints in a 2-D global model formulation in isentropic coordinates. This is the objective of the present study.

In an earlier work (Tung and Yang 1988), some results on Eliassen–Palm flux divergence for October were presented for the southern polar region. The present paper gives a more detailed discussion of the global distribution and seasonal variations of E–P flux divergence and of isentropic mixing coefficient K_{yy}. More importantly, a more comprehensive radiative transfer code is used for the present calculation. The earlier work used the Newtonian cooling approximation.

2. Formulation

To reduce the number of independent variables from four (viz, x, y, z and t) to three (y, z and t), we perform an average over x (longitudes). It is known that significant conceptual differences exist if one chooses potential temperature, instead of the commonly used pressure, as vertical coordinates. The use of potential temperature

$$\theta \equiv T\left(\frac{p_{00}}{p}\right)^{\kappa}$$

as the vertical coordinate has the advantage that, since in the lower stratosphere, large-scale eddy mixing tends

Corresponding author address: Dr. Ka Kit Tung, Dept. of Applied Mathematics, FS-20, University of Washington, Seattle, WA 98195.

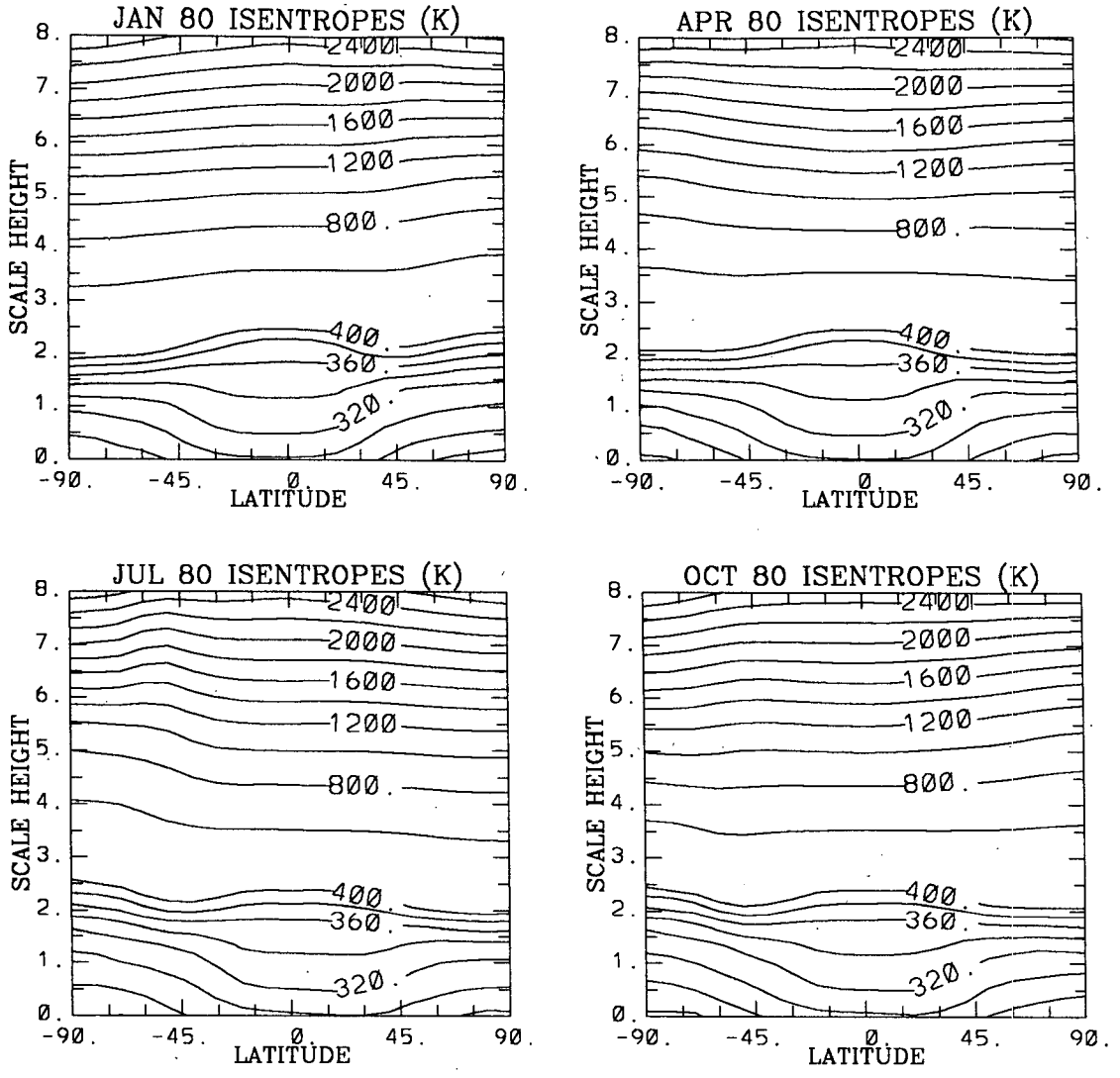

FIG. 1. (a) Potential temperature distribution for 1980 as a function of latitude and pressure. (b) Coordinate surfaces z_1/H as a function of latitude and pressure. The vertical coordinate is $\ln(P_{00}/P)$.

to act predominantly along isentropes (i.e., surfaces of constant θ) (Mahlman et al. 1984; Tung 1984; Plumb and Mahlman 1987), the diffusion tensor can be greatly simplified (Tung 1984). Furthermore, the zonal mean transport velocity, with which tracers and absolute angular momentum are advected, is closely approximated by the Eulerian zonal mean meridional velocity itself (instead of the Lagrangian mean, as is the case in pressure coordinates), when such a zonal average is performed along isentropic surface. [The approximation may become less satisfactory at high latitudes under some circumstances (see Mahlman 1985).] In an isentropic coordinate formulation, the vertical component of the mean advective velocity is in turn given by the thermodynamic equation as simply the zonal mean net diabatic heating rate divided by static stability (Tung 1982, 1984, 1986), without involving mean temperature advection and eddy heat flux terms which are present in a pressure coordinate formulation.

A main disadvantage of adopting the isentropic coordinate system stems from the fact that in the troposphere ($\theta < 350$ K), some isentropes intersect the ground, and they do so more steeply than, for example, the way isobaric surfaces intersect the lower surface (see Fig. 1a). That the ground is far from being a coordinate surface complicates the specification of the lower boundary condition and the treatment of dynamics in the troposphere.

To overcome this problem, Lorenz (1955) suggested that the isentropes be extended "underground," and Andrews (1983) showed how the relevant quantities, such as Eliassen–Palm flux divergence, can be redefined on isentropes that intersect the ground. We have decided, however, against such a remedy, mainly because

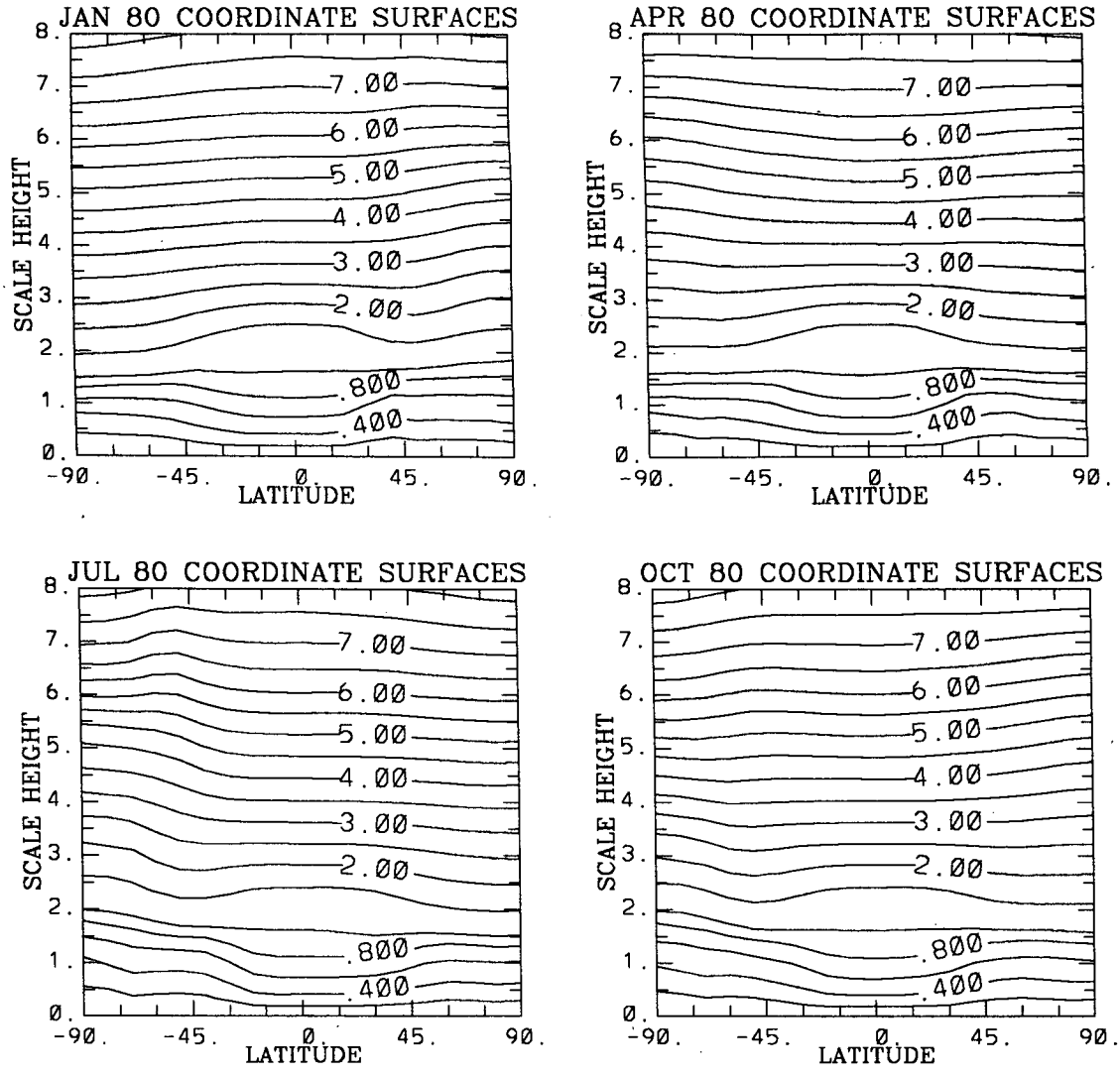

FIG. 1. (*Continued*)

of computational economy. The use of underground isentropes yields a computational domain where a significant portion of grid-points are placed in a region (i.e., underground) with no interesting dynamics. Furthermore, in the kind of data processing that we do in the present work, difficulties may arise in performing zonal averages on those isentropes that are above ground in some longitudes and below ground in others.

Alternatively, the problem of coordinate surface intersecting the ground can be overcome with the adoption of the so-called σ-coordinate, introduced by Phillips (1957) to incorporate the earth's orography into a pressure coordinate system. Thus, with θ/θ_s as the vertical coordinate in a corresponding formulation, the lower surface, $\theta/\theta_s = 1$, is now a coordinate surface, where subscript s denotes the value at the earth's surface. The advantages of isentropic coordinates for the lower stratosphere have now been lost, however, because the coordinate surfaces are no longer isentropes. A compromise is to use a hybrid coordinate system, similar to that adopted in GFDL "SKYHI" model (Fels et al. 1980) except that it is in terms of potential temperature here instead of pressure. We define

$$\frac{z_1}{H} = \frac{\ln(\theta/\theta_0)}{\ln(\theta_c/\theta_0)}, \tag{1}$$

where $H = 7$ km, θ_0 = constant = 263 K for $\theta \geq \theta_c$ and $\theta_0 = \theta_s$ for $\theta < \theta_c$.

The dividing isentrope $\theta_c = 350$ K separates the stratosphere from the "troposphere." For $\theta > \theta_c$, the constant θ_0 is chosen so that $\ln(\theta_c/\theta_0) = \kappa$. Thus

$$\frac{z_1}{H} = \kappa^{-1} \ln(\theta/\theta_0), \tag{2}$$

which is the same as the log-θ coordinate used previously by Holton (1986), and surfaces of constant z_1 correspond to surfaces of isentropes. The equations are the same as in Part I except with $d\theta$ replaced by $\kappa\theta dz_1/H$.

In the troposphere (i.e., $\theta < \theta_c$), the surfaces of constant z_1 are nearly parallel to the contours of the lower surface. In particular, the lower surface, with $\theta = \theta_s$, a variable, corresponds to the coordinate surface $z_1 = 0$ (see Fig. 1b).

For a general z_1, the continuity equation is

$$\frac{\partial}{\partial t}\sigma + \vec{\nabla}_{z_1}\cdot(\sigma\vec{v}) + \frac{\partial}{\partial z_1}(\sigma\dot{z}_1) = 0, \tag{3}$$

where $\sigma \equiv \rho\dfrac{\partial z}{\partial z_1}$ denotes "density" in the z_1-coordinates, $\vec{v}$ the velocity vector, and $\vec{\nabla}_{z_1}$ the horizontal gradient operator holding z_1 constant.

The hydrostatic equation is

$$\sigma = -\frac{1}{g}\frac{\partial p}{\partial z_1} \tag{4}$$

with

$$p = p_{00}\left(\frac{T}{\theta_0}\right)^{1/\kappa}\exp\left\{-\frac{z_1}{H\kappa}\ln\frac{\theta_c}{\theta_0}\right\}. \tag{5}$$

The horizontal momentum equation is

$$\frac{d\vec{v}}{dt} + fk\times\vec{v} = -\vec{\nabla}_{z_1}\Phi + c_pT\left(1-\frac{z_1}{H}\right)\vec{\nabla}_{z_1}\ln\theta_0. \tag{6}$$

The Montgomery streamfunction, Φ, is related to the temperature T as [using (4), (5), and the ideal gas law $p = \rho RT$]:

$$\frac{\partial\Phi}{\partial z_1} = \frac{c_pT}{H}\ln\frac{\theta_c}{\theta_0}. \tag{7}$$

The thermodynamic equation

$$\frac{d\ln\theta}{dt} = \frac{Q}{T},$$

where Q is the net diabatic heating (in K day^{-1}), is expressible as

$$\dot{z}_1 = \frac{H}{\ln(\theta_c/\theta_0)}\left[\frac{Q}{T} + \left(\frac{z_1}{H}-1\right)\frac{d\ln\theta_0}{dt}\right]. \tag{8}$$

At the lower surface, $z_1 = 0$, and $d\ln\theta_0/dt = (Q/T)_s$, so Eq. (8) implies that

$$\dot{z}_1 = 0 \quad \text{at} \quad z_1 = 0. \tag{9}$$

a. Zonally averaged equations

Let an overbar ($\bar{}$) denote zonal average, i.e.,

$$(\bar{}) = \frac{1}{2\pi}\int_0^{2\pi}(\ )d\lambda,$$

while holding y and z_1 constant. λ is longitude; ϕ is latitude; and $y \equiv a\sin\phi$. Let $V\ (=\sigma v\cos\phi)$ and $W\ (=\sigma\dot{z}_1)$ denote the meridional and vertical mass flow rates respectively.

The continuity equation (3) becomes

$$\frac{\partial}{\partial t}\bar{\sigma} + \frac{\partial}{\partial y}\bar{V} + \frac{\partial}{\partial z_1}\bar{W} = 0. \tag{10}$$

The thermodynamic equation (8) becomes

$$\bar{W} \approx \bar{\sigma}\left[\frac{\bar{Q}}{\bar{\Gamma}} + \min\left(0, \frac{z_1}{H}-1\right)\left(\frac{\bar{Q}}{\bar{\Gamma}}\right)_s\right], \tag{11}$$

where

$$\Gamma = \frac{T}{H}\ln\left(\frac{\theta_c}{\theta_0}\right).$$

In the stratosphere, where $z_1/H > 1$, the vertical mass flow rate given by Eq. (11), simplifies to

$$\bar{W} \approx \bar{\sigma}\frac{\bar{Q}}{\bar{\Gamma}}.$$

Note that no eddy heat flux terms appear in the thermodynamics equation for the mean vertical velocity. [The neglected eddy term, $\overline{\sigma'Q'}$, has been shown to be small by Pawson and Harwood (1988); see also Tung (1982).] The only significant eddy driving term would appear in the zonal momentum equation [Eq. (12)].

The x-momentum equation is the same in form as in Part I for $\theta \geqslant 350$ K:

$$\bar{\sigma}\frac{\partial}{\partial t}\bar{L} + \bar{V}\frac{\partial}{\partial y}\bar{L} + \bar{W}\frac{\partial}{\partial z_1}\bar{L} = \square\cdot F, \tag{12}$$

where $L = [u + \Omega a\cos\phi]\cos\phi$ is the absolute angular momentum in the zonal direction, and where $\square\cdot F$ is the Eliassen–Palm flux pseudodivergence defined by

$$\square\cdot F \equiv \frac{\partial}{\partial y}F_y + \frac{\partial}{\partial z_1}F_{z_1} + \frac{\partial}{\partial t}F_t, \tag{13}$$

with

$$F_y = -\overline{V'u'}\cos\phi$$

$$F_{z_1} = -\overline{W'u'}\cos\phi + \frac{\overline{p'}}{g}\frac{\overline{\partial\Phi'}}{a\partial\lambda}$$

$$F_t = -\overline{\sigma'u'}\cos\phi$$

[$(\ )' \equiv (\ ) - (\bar{})$]. It is a *pseudo*divergence $\square\cdot F$, instead of the usual divergence $\nabla\cdot F$, because of the finite amplitude effects included. The extra term, F_t, would be absent if the simple zonal average is replaced by a mass-weighted one (see Part I).

For $\theta \leqslant 350$ K, an extra eddy term,

$$c_p\left(1-\frac{z_1}{H}\right)\overline{T'\frac{\partial}{\partial x}\ln\theta'_s},$$

would appear in the right-hand side of Eq. (13) arising from our "terrain-following" coordinate system. This

term tends to vanish for large-scale thermal patterns where T' and θ_s' are mostly in phase, so we shall neglect it in the following analysis.

Equation (7), when zonally averaged, is

$$\frac{\partial \bar{\Phi}}{\partial z_1} = \frac{c_p \bar{T}}{H} \ln \frac{\theta_c}{\theta_0}. \tag{14}$$

The y-momentum equation is approximated by the following balanced-wind relationship:

$$f\bar{u} + \frac{\bar{u}^2 \tan\phi}{a} = -\frac{1}{a}\frac{\partial}{\partial \phi}\bar{\Phi} + c_p \bar{T}\left(1 - \frac{z_1}{H}\right)\frac{1}{a}\frac{\partial}{\partial \phi}\ln\bar{\theta}_0. \tag{15}$$

The extra term arising from the coordinate transformation cannot be neglected in the troposphere.

b. Strategy for calculating $\square \cdot F$

We shall calculate the left-hand side of the zonal momentum equation [Eq. (12)] using the observed temperature field. The Eliassen–Palm pseudodivergence is then deduced as the amount of zonal force required to maintain the mean zonal momentum budget as observed. This procedure has previously been adopted by Newman et al. (1988), Tung and Yang (1988), Shine (1989), and also discussed previously by Tung (1987).

3. Calculation of Eliassen-Palm flux pseudodivergence

a. Input data

Our diagnostic calculation of the quantity $\square \cdot F$ is independent of the validity or accuracy of the param-

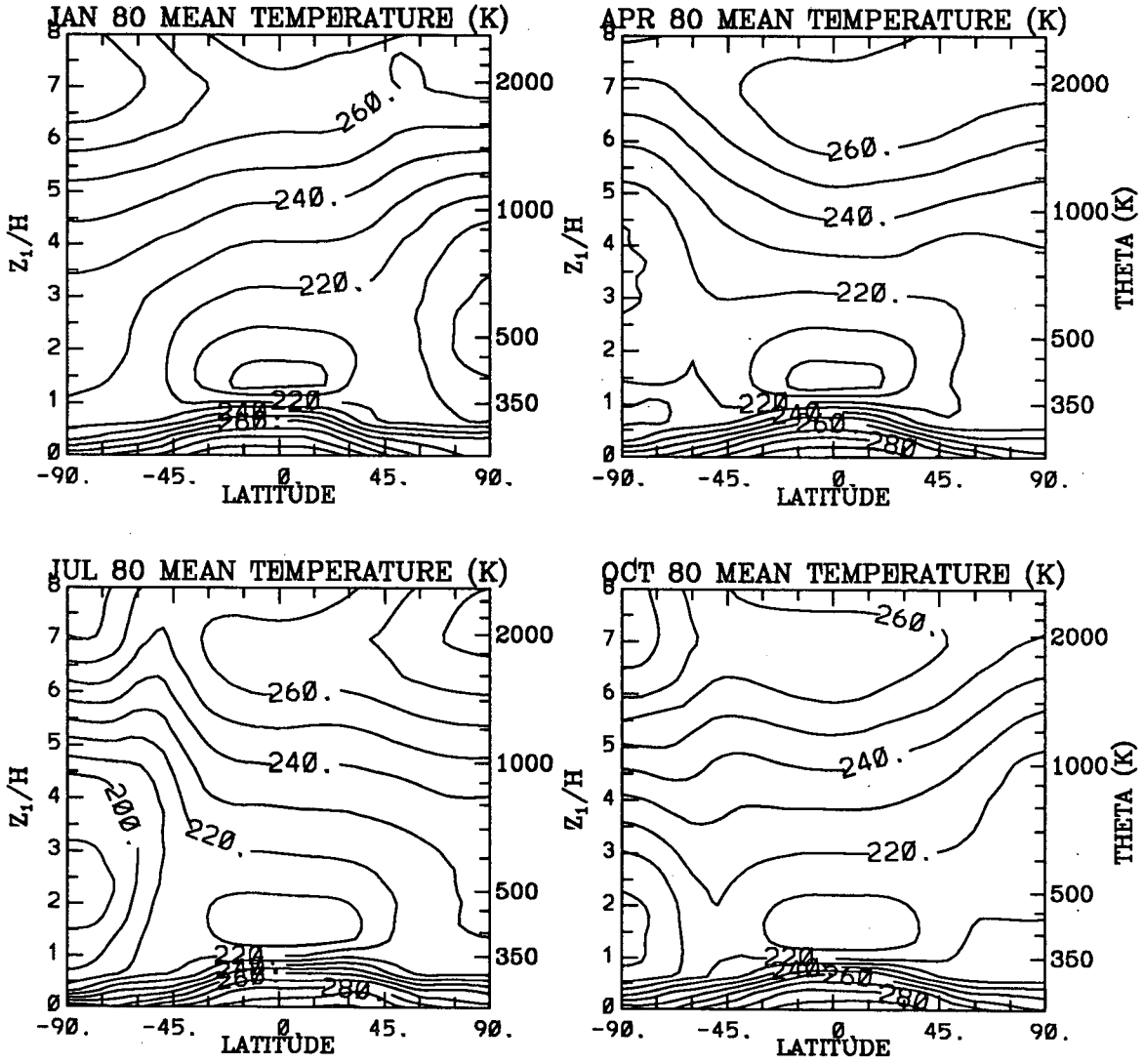

FIG. 2. Observed (NMC) temperatures for 1980 as a function of latitude and potential temperature. The vertical coordinate, z_1/H, is shown in Fig. 1b.

eterization to be introduced in section 4. It is deduced from the zonal mean zonal momentum equation (12) as the amount of wave driving needed to maintain the atmospheric angular momentum at its observed value. Since it is calculated via an evaluation of the left-hand side of (12), however, its accuracy is dependent on the quality of the input data (e.g., the observed values of zonal mean temperature and zonal mean ozone fields), and on the accuracy of the radiative transfer code used to calculate the diabatic heating rate. The reliability of both is less than desired, and this fact should be kept in mind in any quantitative discussion of the resulting product.

The observed NMC daily temperature field in *three dimensions* from surface to about eight scale heights is kindly provided to us by David Wu and Eric Nash of NASA. The 3-D data are zonally averaged *on surfaces of constant potential temperature* above $\theta = 350$ K, and on surfaces of constant z_1 below. The zonally averaged temperature field is shown in Fig. 2, and generally the large scale features are not too different from the temperature field averaged on isobaric surfaces (see Geller and Wu 1987), except for the compressed shape of troposphere due to our choice of coordinates. High frequency variations are filtered out using Fourier analysis in both space and time to facilitate the derivative operations. A total number of 19 (horizontal) $\times$ 25 (vertical) $\times$ 37 (temporal) cosine coefficients are used for each year in our model calculations.

In addition to temperature field, ozone, and to a less extent, other radiatively active gases, are needed as input to the radiative transfer calculations. McPeters et al. (1984) presented zonal mean ozone mixing ratios as a function of latitude and height for four months in 1979 based on SBUV data (shown in Fig. 3).

Rosenfield et al. (1987) have used this observed ozone field along with the observed NMC temperature field in their radiative transfer calculations and found

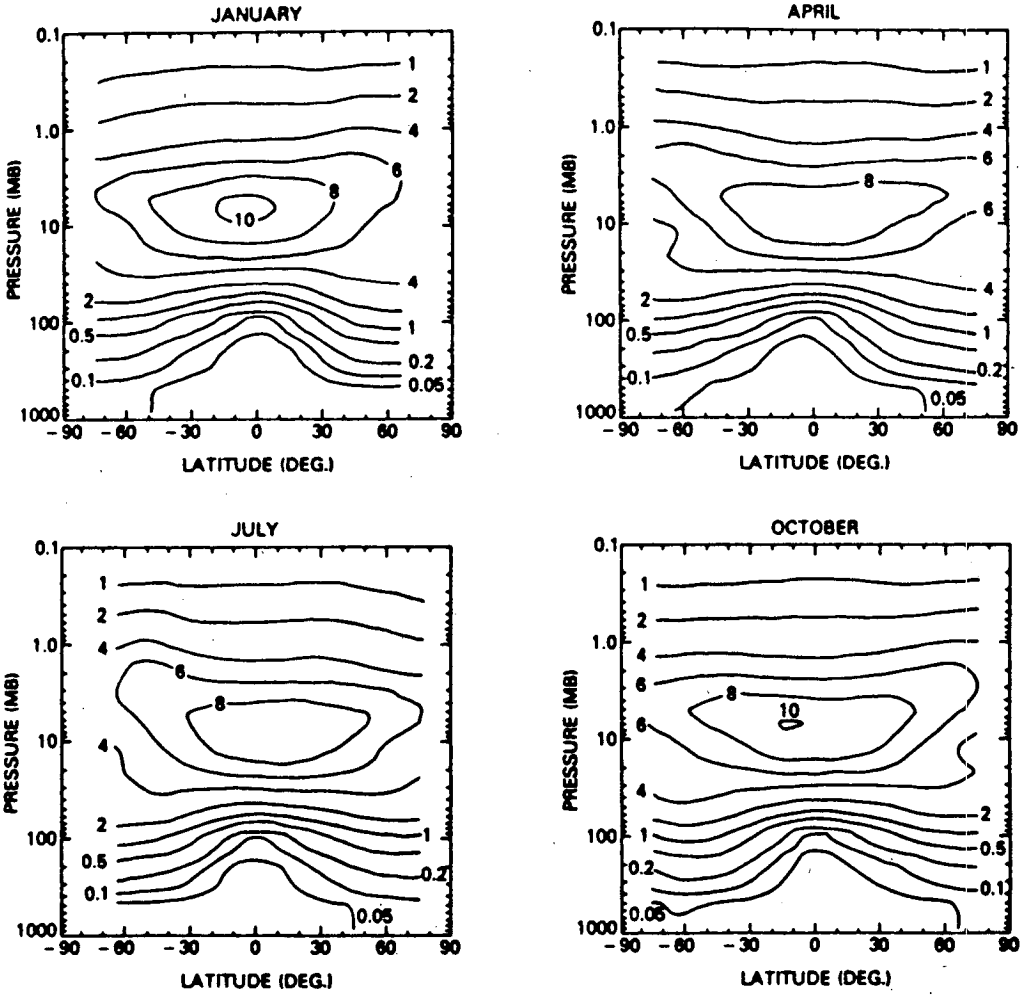

FIG. 3. Observed (SBUV) ozone distribution for 1979 as a function of latitude and pressure, taken from McPeters et al. (1984).

large imbalances in the calculated net radiative heating rates. Similar problems were reported by other authors using LIMS data (e.g., Kiehl and Solomon 1986; Callis et al. 1987; Shine 1989). The imbalances are presumably due to errors in the observed data, in ozone and possibly in temperature, and to the uncertainties in the radiative calculations.

From a technical point of view, the imbalance implies, aside from the uncertainties in the radiative transfer codes, that the SBUV (or LIMS) ozone field is incompatible with the NMC (or LIMS) temperature field, and, if these are used in a diagnostic calculation in our model, mass cannot be conserved. To circumvent this problem, we have decided to use model-produced ozone field (shown in Fig. 4) as a substitute for the observed data. The details of the ozone model will be described in a future paper. It suffices for our present purpose to point out that the model-produced ozone field is strictly compatible with the input NMC temperature field at any time in the sense that it is produced under exact mass conservation. It is furthermore very similar to the SBUV data, as can be seen by comparing Fig. 4 with Fig. 3. One could regard Fig. 4 as the observed ozone field "objectively assimilated" by the model.

In regions above 40 km, where ozone is mostly in photochemical equilibrium, mass conservation cannot be strictly enforced by dynamical redistribution. Here the imbalance in $\bar{Q}$ is simply subtracted uniformly from the deduced value for $\bar{Q}$. The same procedure is also applied to the troposphere, where ozone plays a minor role in the radiative budget.

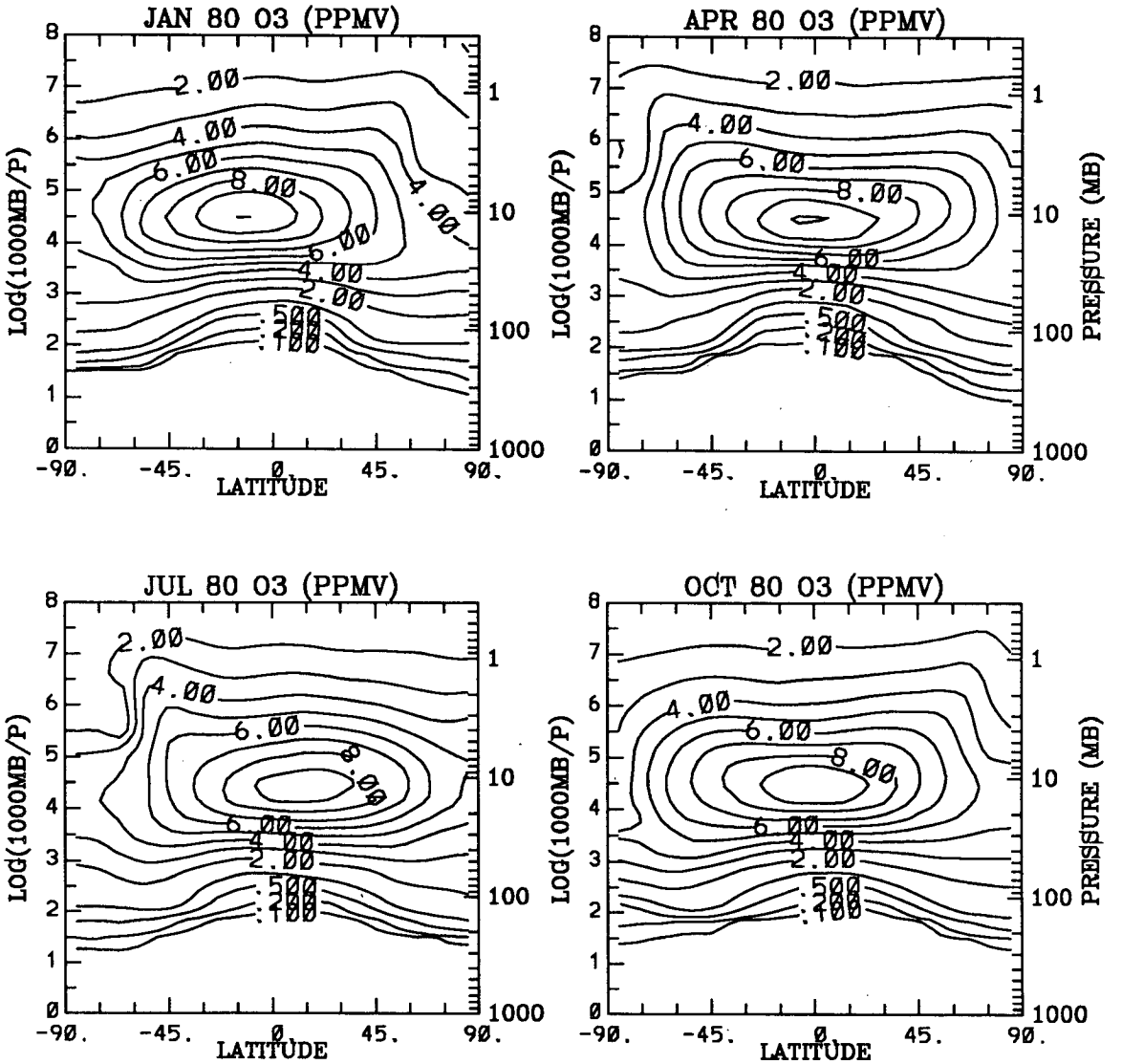

FIG. 4. Model simulated ozone distribution for 1980 as a function of latitude and pressure.

Water vapor field is taken from LIMS and methane is taken from SAMS.

b. Calculation of $\bar{Q}$

An earlier version of $\bar{Q}$ calculated using Newtonian cooling parameterization appeared in Tung and Yang (1988). The present result is calculated using a comprehensive radiative transfer code.

The radiative transfer code used is a fast quasi-narrowband model documented in Olaguer and Yang (1989). For our purpose here, only the product—the net diabatic heating rate $\bar{Q}$—will be used, and this is displayed in Fig. 5. A comparison with line-by-line calculations shows that errors are less than 10% throughout the domain considered here. In most regions, the error is less than 5%. The main features of the net heating rate is broadly consistent with those obtained by previous authors (e.g., see Rosenfield et al. 1987). It consists of net heating in the summer stratosphere and mesosphere (above about 30 km) and net cooling in the winter hemisphere. In the lower stratosphere there is net heating in the equatorial region and cooling over both poles. The magnitude of the net heating in the equatorial lower stratosphere is, however, somewhat smaller than that of Rosenfield et al. (1987). The reasons for the difference are discussed in Olaguer and Yang (1989).

c. The diabatic circulation

The diabatic circulation deduced from $\bar{Q}$ using the thermodynamic equation (11) and the continuity

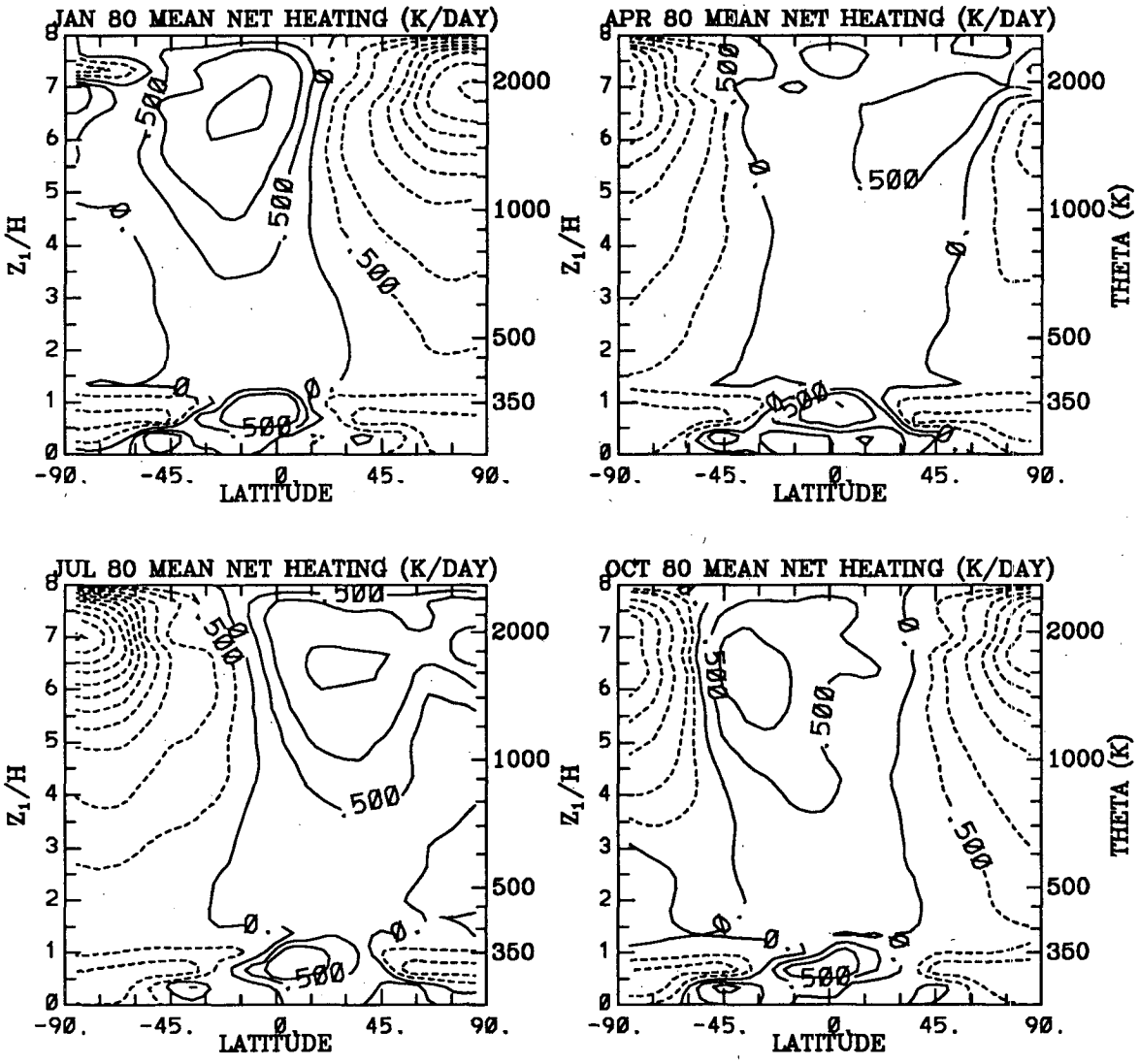

FIG. 5. Calculated diabatic heating rate $\bar{Q}$ as a function of latitude and potential temperature. The vertical coordinate, z_1/H, is shown in Fig. 1b. Contour values: ± 0, 0.5, 1, 2, 3, ...

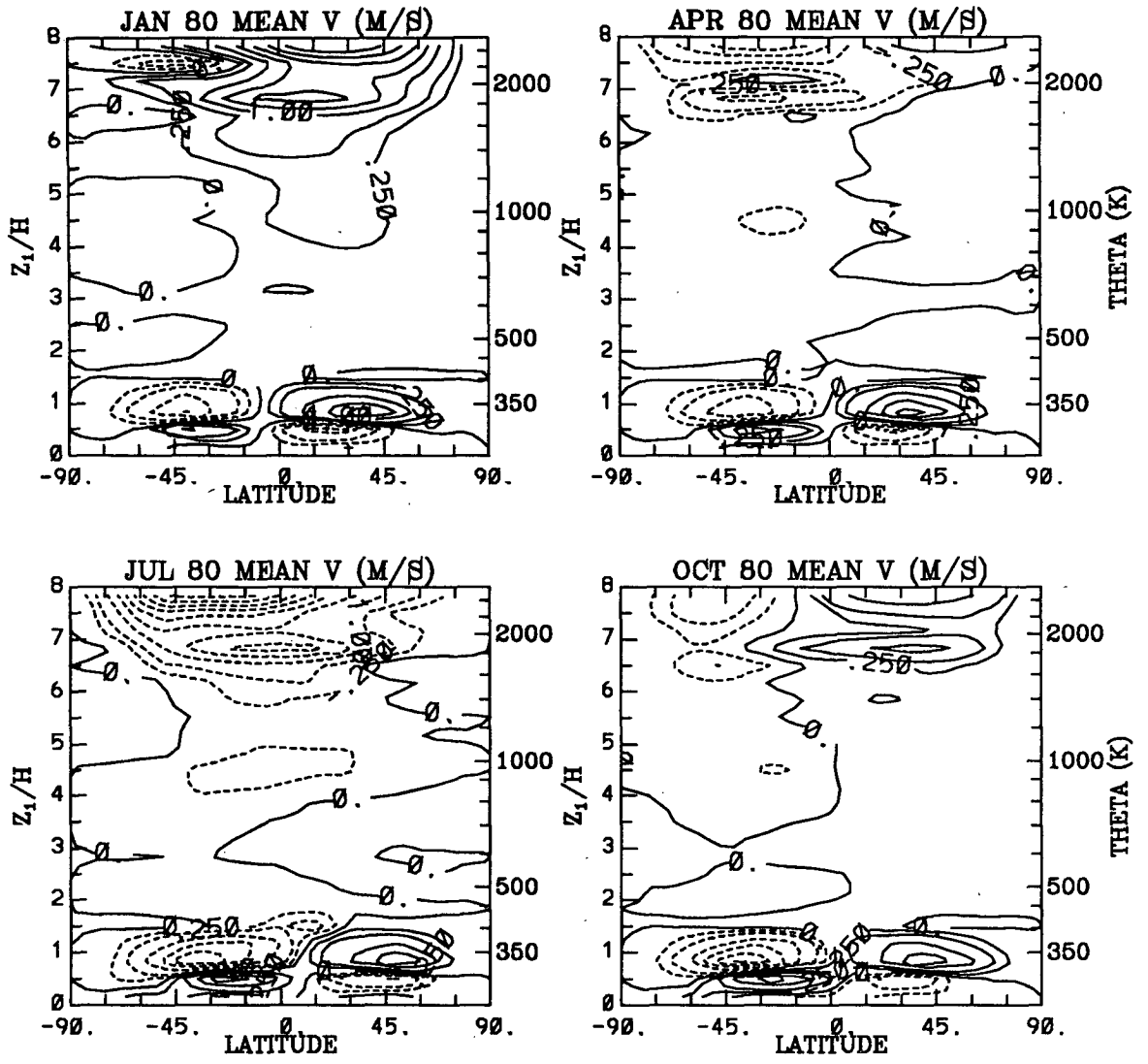

FIG. 6. Calculated meridional velocity $\bar{V}/\sigma$ as a function of latitude and potential temperature. The vertical coordinate, z_1/H, is shown in Fig. 1b. Contour values: ±0, 0.25, 0.5, 1, 1.5, 2, ...

equation (10) is shown in Fig. 6 for the meridional velocity $\bar{V}/\bar{\sigma}$, in Fig. 7 for the vertical velocity $\bar{W}/\bar{\sigma}$, and in Fig. 8 for the vector field $(\bar{V}, \bar{W})$. Figure 8 shows a two-cell diabatic circulation in the lower stratosphere, with rising motion in the equatorial region and sinking motion over both summer and winter poles, with the winter circulation being stronger than the summer circulation. Above about 25 km, the two-cell pattern changes to a pole-to-pole circulation, with upwelling in the summer hemisphere and subsidence in the winter hemisphere. These features of the diabatic circulation have been pointed out previously by Murgatroyd and Singleton (1961), Dopplick (1972, 1979), Dunkerton (1978), Tung (1982), Kiehl and Solomon (1986), Rosenfield et al. (1987), Callis et al. (1987), and, Pawson and Harwood (1989).

d. Calculation of E–P flux divergence

Using the zonal mean momentum equation (12) we now deduce the net wave forcing that maintains the observed angular momentum budget.

First, we deduce the zonal winds $\bar{u}$ from the NMC temperature $\bar{T}$, using the balanced-wind relationship (15), assuming $\bar{u} = 0$ at the surface. Like geostrophic approximation, balanced-wind relationship breaks down near the equator. Zonal winds within ±20° of equator are linearly interpolated using values at ±20°. This procedure is somewhat arbitrary and has the possibility of underestimating the equatorial easterlies under equinox conditions. (Ideally, a dataset for $\bar{u}$, if available, would have eliminated these problems.) The deduced E–P flux divergence and mixing coefficient,

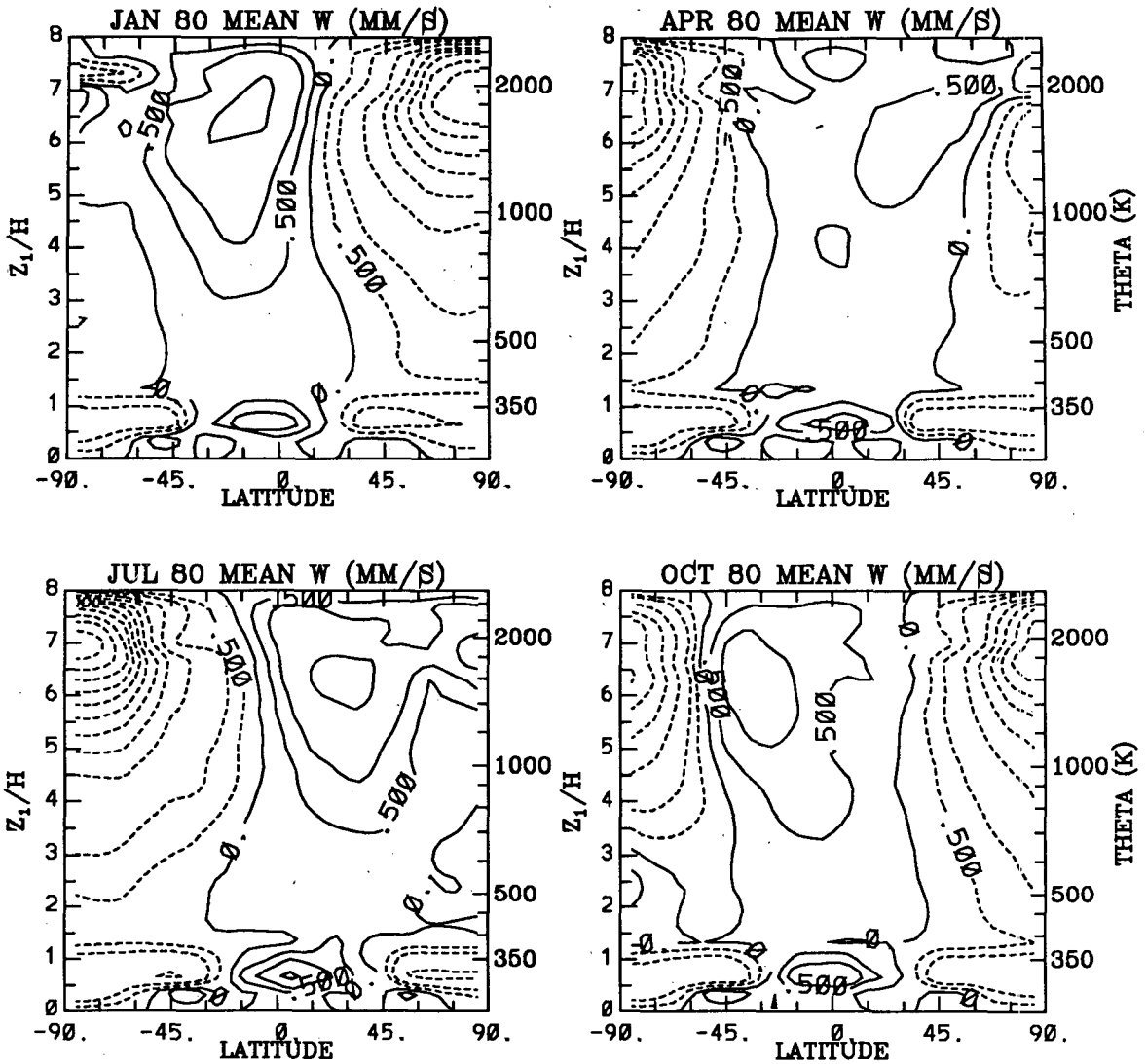

FIG. 7. Calculated vertical velocity $\bar{W}/\sigma$ as a function of latitude and potential temperature. The vertical coordinate, z_1/H, is shown in Fig. 1b. Contour values: ±0, 0.5, 1, 2, 3, ...

using present procedure, suffer larger uncertainties and are probably not very reliable at equatorial regions. Near the poles, the quadratic equation (15) for $\bar{u}$ may have no real solutions at some isolated locations, and values at these locations are extrapolated. For the purpose of calculating zonal winds, high resolution temperature data is used. Then the zonal winds are smoothed by retaining the same number [19 (horizontal) × 25 (vertical) × 37 (temporal)] of Fourier coefficients as temperature for subsequent model calculations. The resulting fields are shown in Fig. 9.

From zonal wind $\bar{u}$, we can easily calculate the absolute angular momentum $\bar{L}$ and its time rate of change. With ($\bar{V}$, $\bar{W}$) already determined, and density $\bar{\sigma}$ obtained from (4), the left-hand side of Eq. (12) is known. Thus $\Box \cdot F$ is obtained. The quantity $\Box \cdot F/\bar{\sigma}$, in unit of acceleration (force per unit mass), is shown in Fig. 10. Note that no parameterization scheme has been adopted so far and the $\Box \cdot F/\bar{\sigma}$ calculated represents net wave forcing, including planetary, gravity and equatorial waves (and possibly small-scale damping).

The results show, as generally expected, that wave forcing tends to decelerate the zonal mean jets. In January, the stratospheric westerly jet in the Northern Hemisphere experiences a westerly deceleration (as indicated by negative E–P flux divergence). The same is true for the westerly subtropical jet in both hemispheres in the upper troposphere and lower stratosphere.

It is interesting to note that the dipole structure of the E–P flux divergence centered near the tropospheric jet maxima in both hemispheres. It appears to imply a wave deceleration above the jet maxima, but a wave *acceleration* below the jet core. The latter is probably necessary for the maintenance of the zonal jets against surface drag and mountain torque in the lower atmosphere. Fritts et al. (1989) presented measurements,

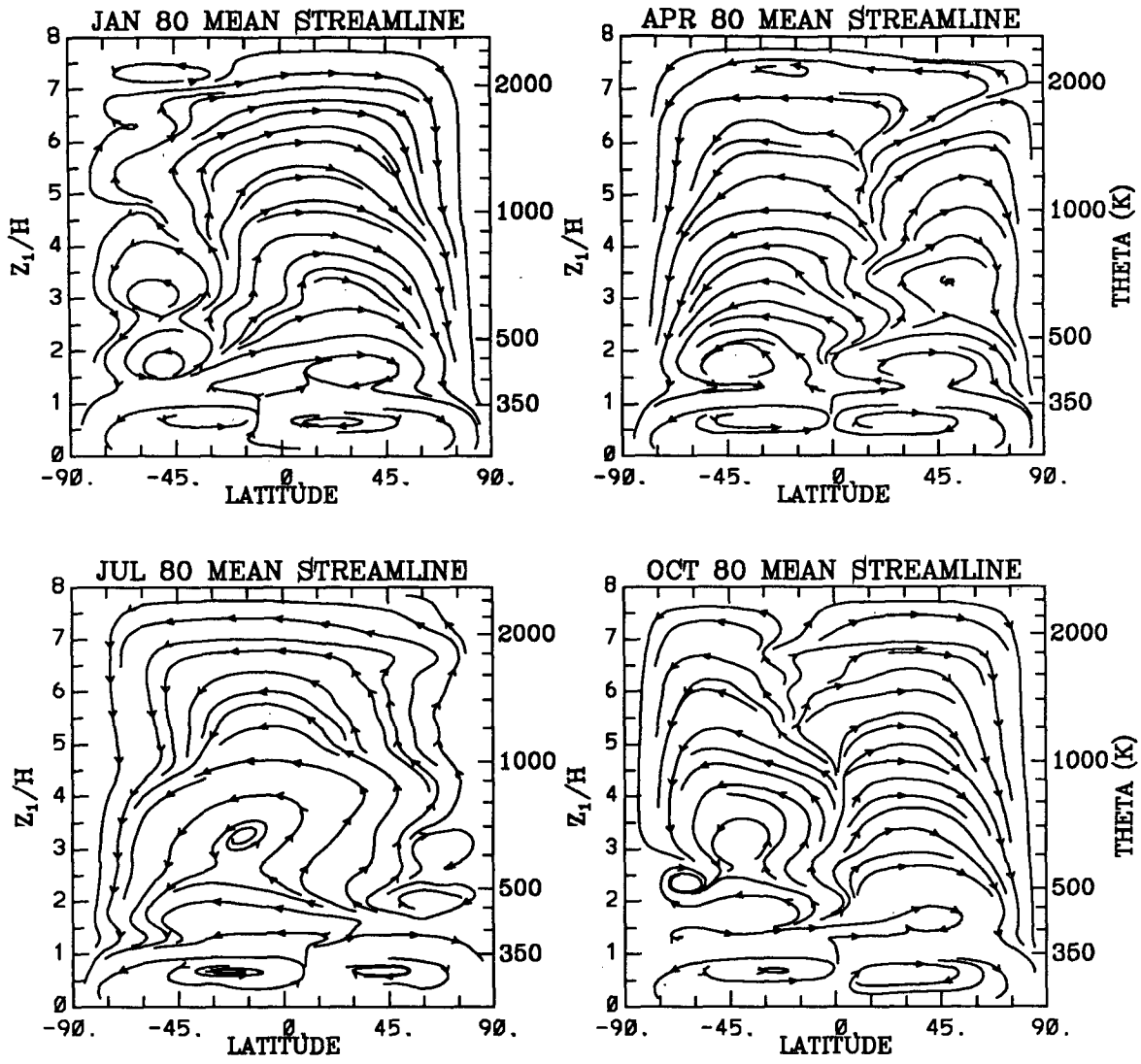

FIG. 8. Streamlines for vector field $(\bar{V}, \bar{W})$ as a function of latitude and potential temperature. The vertical coordinate, z_1/H, is shown in Fig. 1b.

using MU radar, of gravity wave momentum fluxes in Shigaraki, Japan, and showed that in the troposphere the gravity wave momentum flux divergence resulted in an acceleration below the jet core and a deceleration above it of about 1–2 m s^{-1} day^{-1}. Our dipole structure in E–P flux divergence mentioned earlier is consistent with this interpretation of Fritts et al. (1989). The magnitude of the deceleration and acceleration is found here to be 3 to 4 times larger, however. Large uncertainty exists in the treatment of latent heating in the troposphere. We have performed another calculation using a smaller latent heating. The dipole structure remains, but the magnitude of the deceleration and especially acceleration is reduced by up to a factor of 2. The same dipole patterns are also found in the "SKYHI" general circulation model (Mahlman and Umscheid 1984).

The easterly jet in the summer hemisphere experiences an easterly deceleration (or westerly acceleration, as indicated by positive E–P flux divergence) above 40 km. This is probably effected through the drag caused by breaking gravity waves which have westerly phase speeds (Lindzen 1981). Stationary planetary waves probably cannot penetrate above the 40 km region in an easterly flow.

In July, the winter and summer hemispheres reverse. Westerly jet experiences a westerly deceleration and easterly jet experiences an easterly deceleration as in January, except that the westerly deceleration is slightly weaker. Consequently the westerly jets in the Southern Hemisphere winter are stronger than their Northern Hemisphere counterparts.

The typical magnitude of E–P flux divergence in the stratosphere is about 1 to 2 $\times 10^{-5}$ m s^{-2} for all seasons,

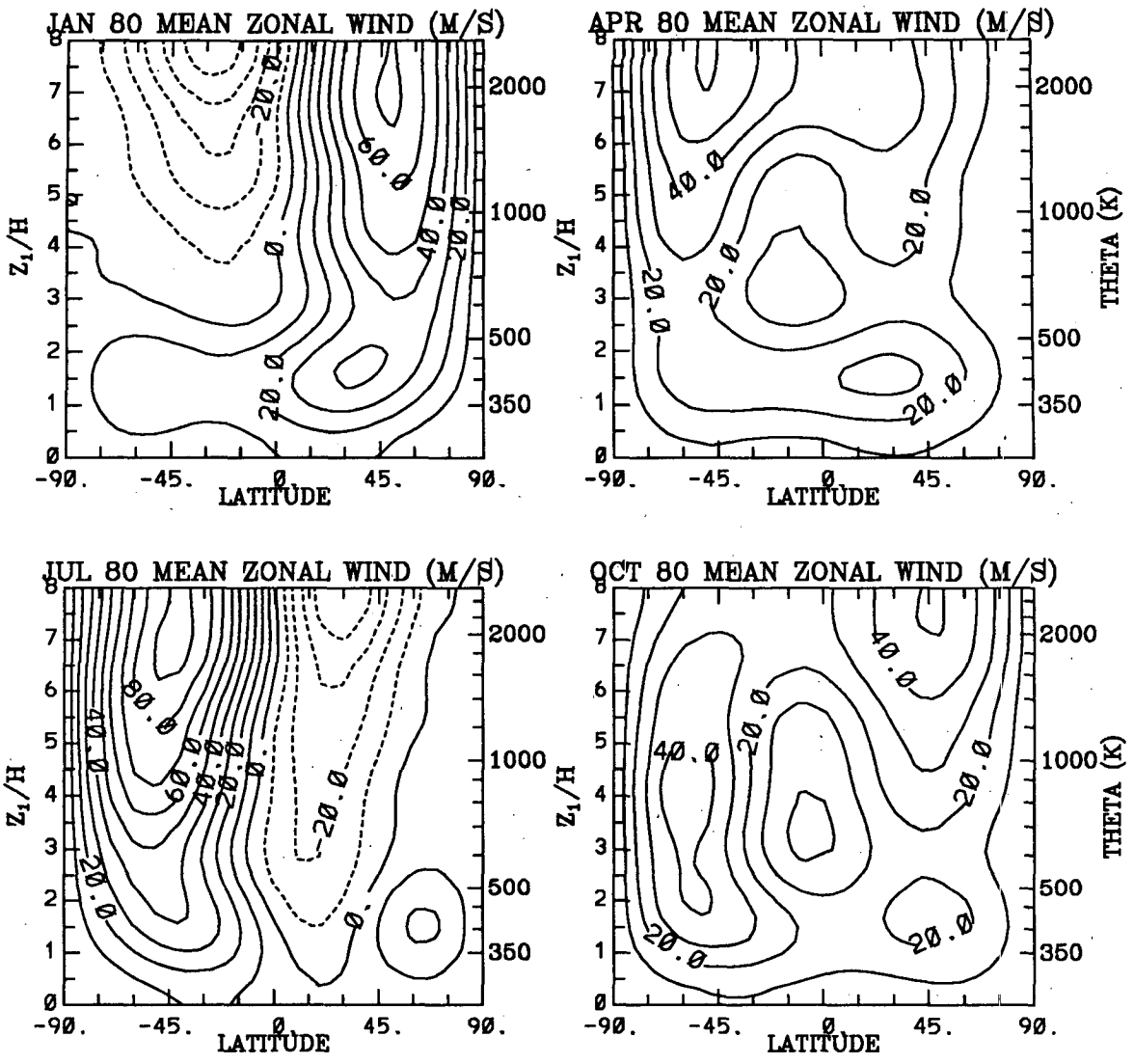

FIG. 9. Zonal wind, deduced from the temperature shown in Fig. 2 using the balanced-wind relationship, as a function of latitude and potential temperature. The vertical coordinate, z_1/H, is shown in Fig. 1b.

representing a deceleration of the zonal jets of about 1 m s^{-1} per day. Larger magnitude is found in upper stratosphere and lower mesosphere, indicating stronger wave dissipation there, which causes the jets to close. A significant contribution to the E–P flux divergence should probably be attributed to the breaking gravity waves there.

Sizable regions of divergence of E–P flux in January winter stratosphere found in Geller et al. (1983) are not present in our results; the discrepancy is perhaps due to the difference between quasi-geostrophic and primitive forms of the E–P flux divergence as pointed out by Robinson (1986), and to satellite data quality for the eddy components. Regions of divergence of E–P flux remains in July winter stratosphere, but the magnitudes are much weaker than those reported by Hartmann et al. (1984).

The pattern and magnitude of the E–P flux divergence in the stratosphere in the January Northern Hemisphere are remarkably similar to those obtained from GCM simulation of Mahlman and Umscheid (1984). The latter included a small spot of positive E–P flux divergence at 40 km level. Our calculation indicates that this spot appears occassionally on a daily time scale, but disappears on a monthly mean basis. Our "spot" for Southern July latitudes, however, is more persistent and occupies a larger area than for our Northern January latitudes. In this respect, our July southern latitudes are more similar to the GCM January northern latitudes. Our E–P flux divergence in January has a somewhat larger magnitude (by a factor of 2, more deceleration) in the 30–40 km region than that in the GCM; the latter is missing a secondary maximum in $(-\nabla \cdot F)$ in this region.

4. Parameterization of Eliassen–Palm flux pseudodivergence

In the following discussion, we shall restrict our attention to $\theta > 350$ K. Parameterization for the troposphere is more problematic and will not be done in detail. The treatment adopted for the troposphere in the present work will be discussed later.

a. Relationship between the E–P flux pseudodivergence and Ertel's potential vorticity flux

The general relationship between the E–P flux pseudodivergence and the flux of Ertel's potential vorticity can be written as [see Eq. (4.6) of Part I]:

$$\Box \cdot F = \bar{\sigma}\overline{(\sigma P^*)v^*}\cos\phi - \bar{\sigma}\dot{\theta}^*\frac{\partial u}{\partial \theta}, \qquad (16)$$

where

$$P \equiv \frac{\zeta + f}{\sigma}$$

is Ertel's potential vorticity and

$$h^* \equiv h - \hat{h},$$
$$\hat{h} \equiv \overline{\sigma h}/\bar{\sigma}.$$

For large-scale Rossby waves, the last diabatic term in Eq. (16) is smaller than the first adiabatic term on the right-hand side by one to two orders of magnitude (see Part I). So

$$\Box \cdot F \approx \bar{\sigma}\overline{(\sigma P^*)v^*}\cos\phi \qquad (17)$$

for Rossby waves and other eddies that mix predominantly along (rather than across) isentropes.

For radiatively damped equatorial Kelvin waves, which have negligible meridional displacements, the last term in (16) may become important if Kelvin waves are considered in isolation. In the easterly portion of the stratosphere (above 40 km during summer), the adiabatic term is small due to a lack of planetary wave penetration. Here the deceleration of the easterly jet found in section 3 should be attributed to the breaking gravity waves (Lindzen 1981). The same should be true near the tropospheric jet core region (Fritts et al. 1989).

The exact equation of motion satisfied by the Ertel's potential vorticity in the presence of diabatic effects can be derived from the vorticity equation (Haynes and McIntyre 1987):

$$\frac{\partial}{\partial t}(\vec{\nabla}\theta \cdot \vec{\zeta}_a) + \vec{\nabla}\cdot[(\vec{\nabla}\theta \cdot \vec{\zeta}_a)\vec{v} - \dot{\theta}\vec{\zeta}_a] = 0, \qquad (18)$$

where $\vec{\nabla}$ is the three-dimensional gradient operator, and $\vec{\zeta}_a = 2\vec{\Omega} + \vec{\nabla} \times \vec{v}$ is the three-dimensional absolute vorticity. If Eq. (18) is specialized to the θ-coordinate system, then the vertical component of the vector flux in (18) cancels (Haynes and McIntyre 1987). Thus

$$\frac{\partial}{\partial t}(\zeta_{a\theta}) + \vec{\nabla}_\theta \cdot [(\zeta_{a\theta})\vec{v} - \dot{\theta}\vec{\zeta}_a] = 0,$$

where

$$\zeta_{a\theta} = f + \zeta = 2\Omega \sin\phi + \frac{\partial}{\partial x}v - \frac{\partial}{\partial y}(u\cos\phi)$$

is the vertical component of the absolute vorticity vector. [$y \equiv a\sin\phi$, $\partial/\partial x \equiv 1/a\cos\phi(\partial/\partial\lambda)$, and $\vec{\nabla}_\theta$ is the horizontal gradient operator holding θ constant.] But since the Ertel's potential vorticity P is defined as $P = \zeta_{a\theta}/\sigma$, we have

$$\frac{\partial}{\partial t}(\sigma P) + \vec{\nabla}_\theta \cdot [\sigma P\vec{v} - \dot{\theta}\vec{\zeta}_a] = 0. \qquad (19)$$

Equation (19) is the statement that even for the general nonconservative case, Ertel's potential vorticity behaves like a conservative tracer (with no sources and sinks) whose flux is directed only along isentropic surfaces (Haynes and McIntyre 1987); however, its isentropic flux is not simply the product of the isentropic velocity and itself, as flux of a tracer is normally defined, but rather this product plus $-\dot{\theta}\vec{\zeta}_a$, for the general diabatic case. Haynes and McIntyre (1987) showed that this last term is small under geostrophic scaling. It should also be small in the general (nongeostrophic) case provided that we are considering the geophysical case of a shallow layer of fluid. In fact, its horizontal gradient is of the same order as the acceleration term proportional to the horizontal component of the absolute vorticity vector, which is commonly neglected in the *primitive* equations. [This term was neglected in Eq. (5.1) of part I.] Thus, (19) can be approximated by

$$\frac{\partial}{\partial t}(\sigma P) + \vec{\nabla}_\theta \cdot (\sigma P\vec{v}) = 0, \qquad (20)$$

the same as in the adiabatic case. The approximation may not be valid for smaller scale waves whose ratio of vertical to horizontal scales does not scale with H/a.

The above discussion suggests that the Ertel's potential vorticity is perhaps the ideal tracer that one can use to deduce the isentropic mixing coefficient, for both the adiabatic and diabatic cases, provided that the formulation is expressed in isentropic coordinates. In pressure coordinates, for example, vertical flux of P must be retained (see Tung 1984).

b. Closure scheme

The flux of a tracer is usually assumed to be related to its mean gradient through the so-called flux–gradient relationship (Lettau 1951; Reed and German 1965; Green 1970). The validity of such a relationship can be shown mathematically only under the small amplitude assumption (see Plumb 1979; Matsuno 1980;

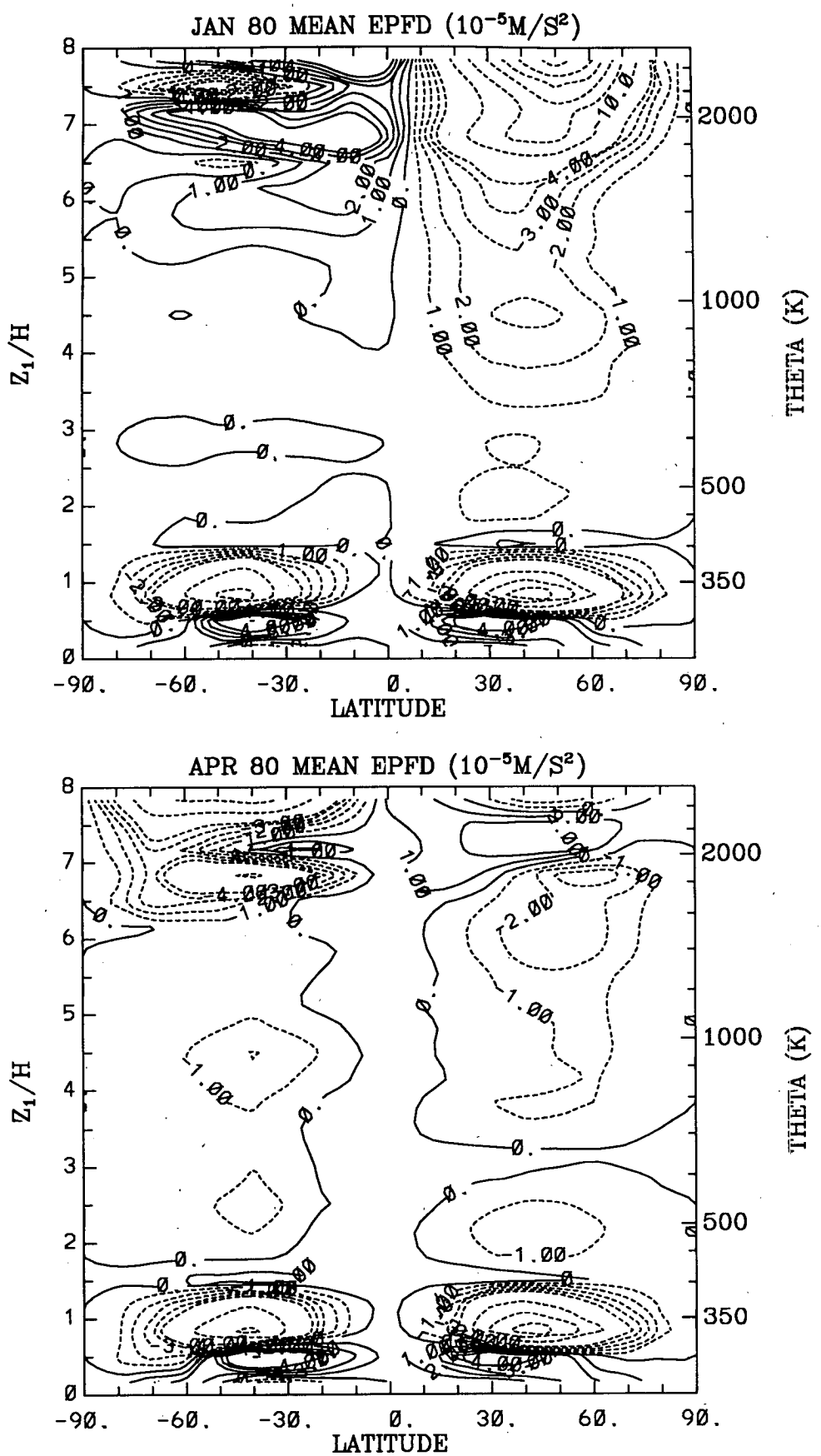

FIG. 10. Calculated Eliassen–Palm flux pseudodivergence as a function of latitude and potential temperature for 1980. The vertical coordinate, z_1/H, is shown in Fig. 1b. Contour values: ±0, 1, 2, 3, 4, 5, 10, 15, . . . (a) for January; (b) for April; (c) for July; (d) for October.

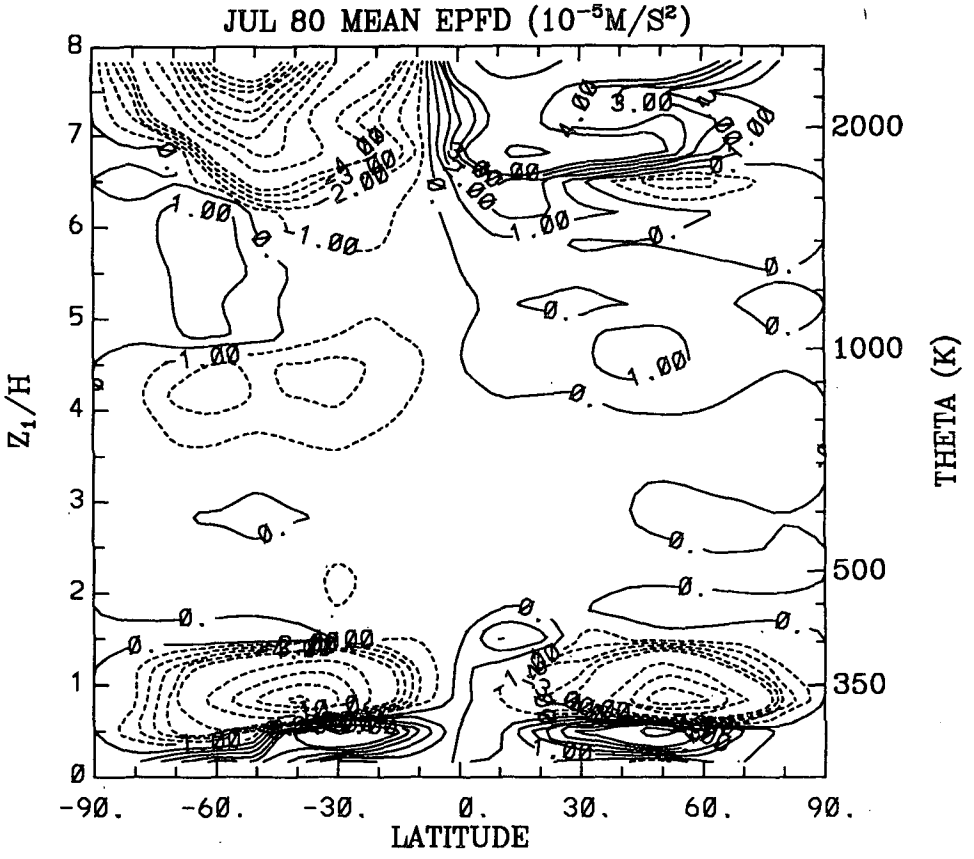

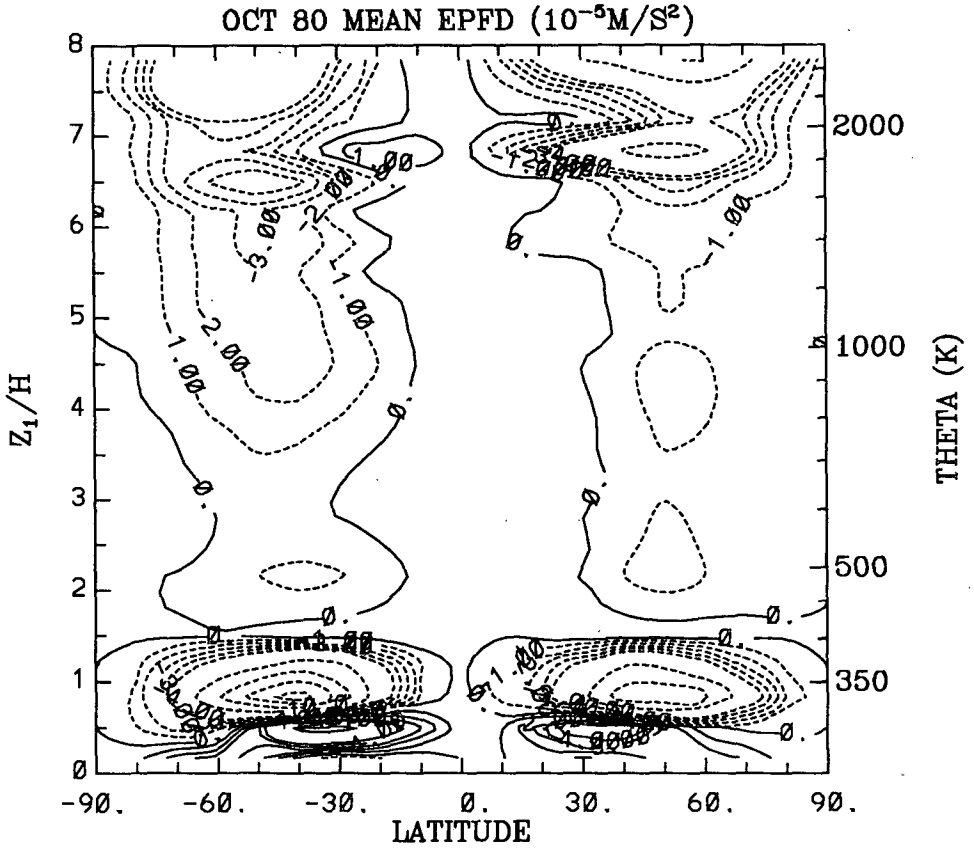

FIG. 10. (*Continued*)

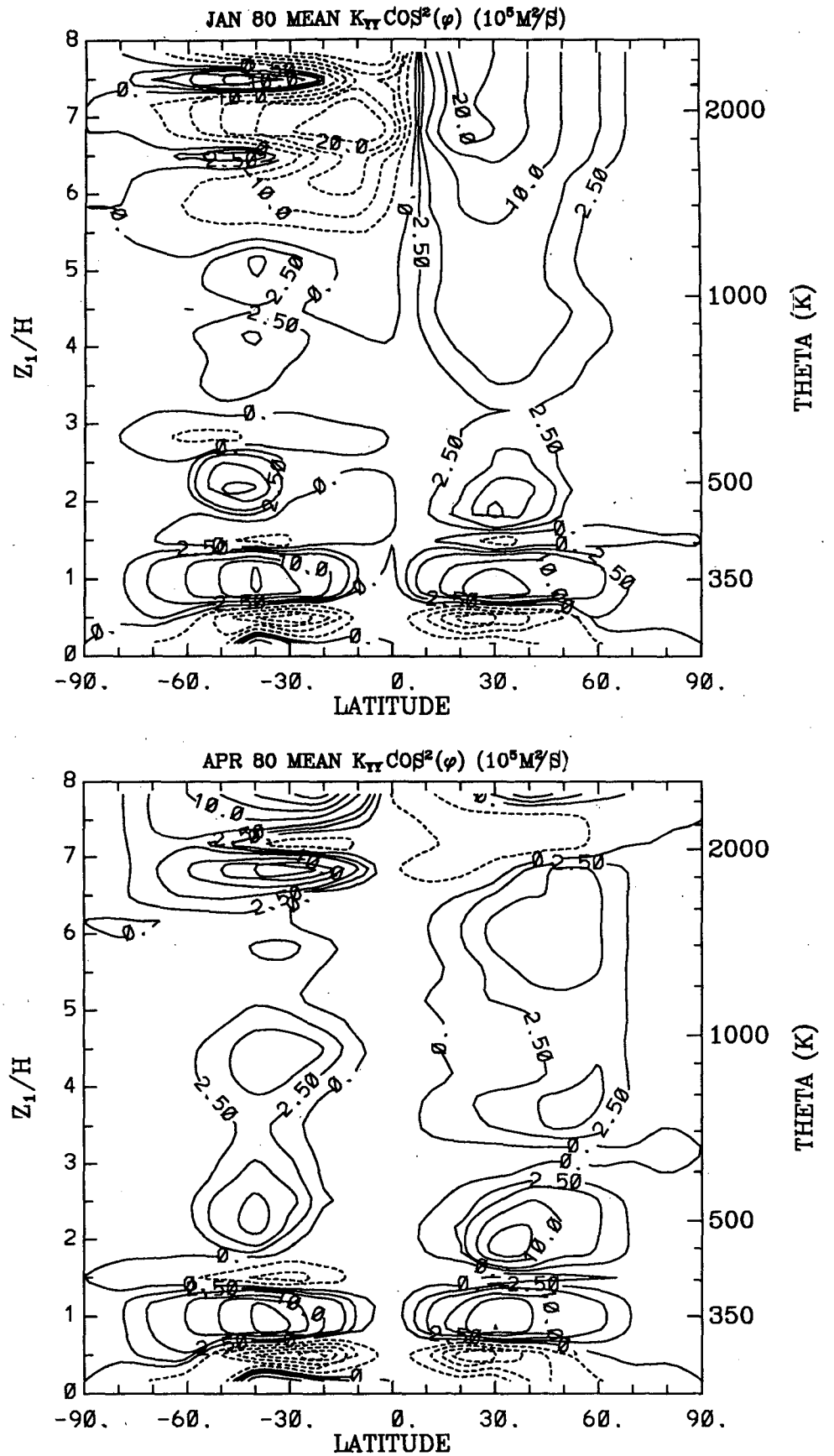

FIG. 11. Calculated isentropic mixing coefficient, $K_{yy}\cos^2(\phi)$, as a function of latitude and potential temperature for 1980. The vertical coordinate, z_1/H, is shown in Fig. 1b. Contour values: 0, 2.5, ±5, ±10, ±15, . . . (a) for January; (b) for April; (c) for July; (d) for October.

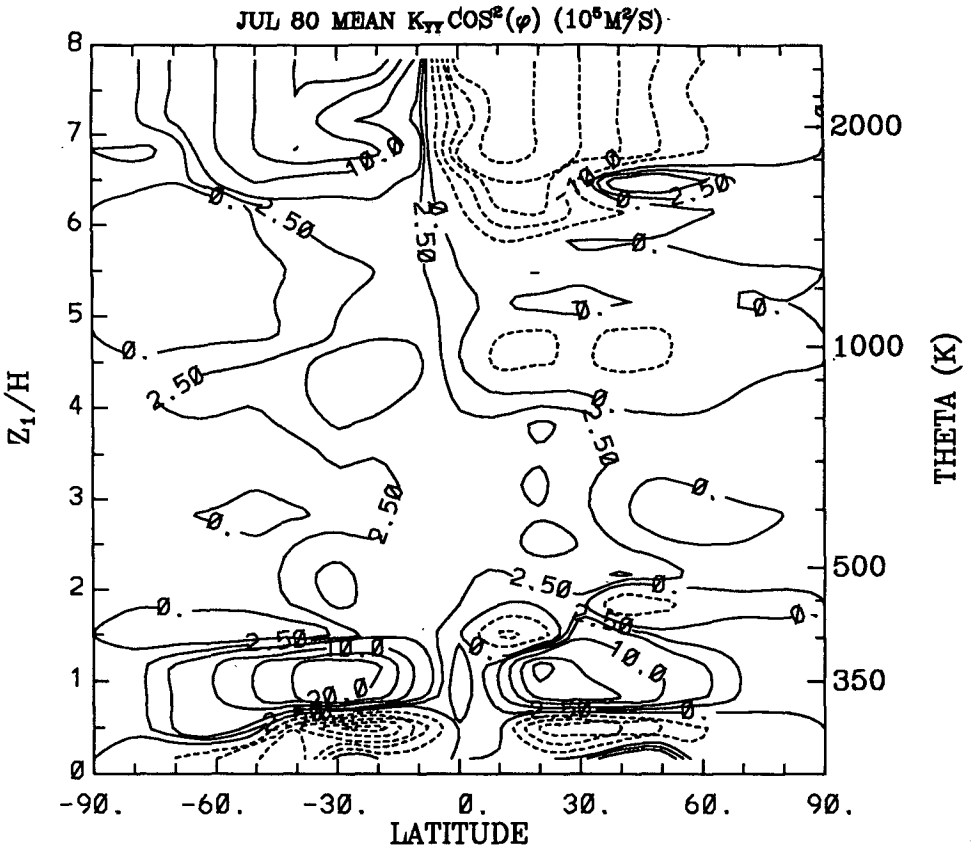

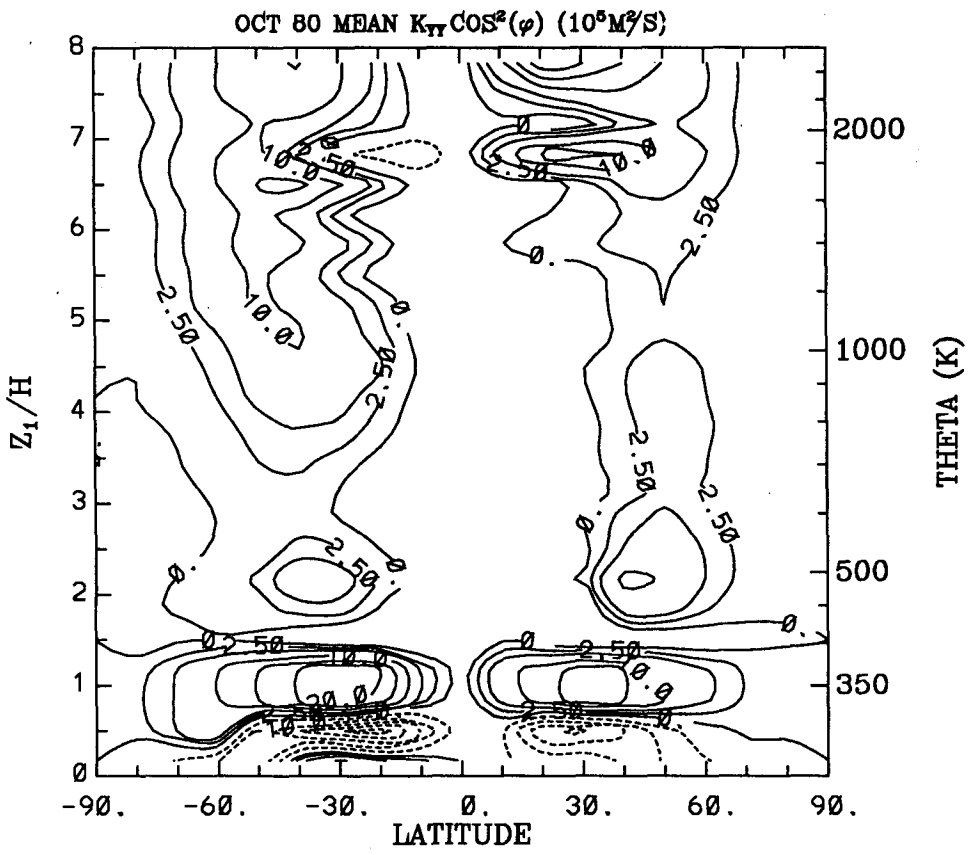

FIG. 11. (*Continued*)

Holton 1980, 1981; Danielsen 1981; Tung 1982, 1984). Using a GCM, Plumb and Mahlman (1987) demonstrated that the flux–gradient relationship also appears to hold approximately for finite amplitude waves, although the amplitude of model waves are probably not as large as that in the real atmosphere.

If we treat Ertel's potential vorticity as a tracer satisfying Eq. (20) (i.e., quasi-adiabatic), the flux–gradient parameterization yields (see Part I):

$$\overline{(\sigma P^*)v^*}\cos\phi = -\bar{\sigma}K_{yy}\cos^2\phi\,\frac{\partial}{\partial y}\hat{P}. \qquad (21)$$

The parameter K_{yy} is the so-called isentropic mixing coefficient given by

$$\bar{\sigma}K_{yy} = \overline{\sigma\frac{\partial}{\partial t}\frac{1}{2}\eta^{*2}}, \qquad (22)$$

where η^* is the eddy meridional displacement. The use of another identity,

$$\bar{\sigma}\hat{P} \equiv f + \bar{\zeta} \equiv -\frac{\partial \bar{L}}{\partial y}, \qquad (23)$$

then completes the parameterization of the eddy forcing term in the zonal mean equation for $\bar{L}$ [Eq. (12)].

Since the focus of the present study is not the troposphere, we have not attempted a detailed parameterization of the tropospheric mixing processes. We have simply extended our stratospheric results downward assuming mixing to occur along surfaces of constant z_1, which in the troposphere are approximately parallel to the lower surface.

5. Calculation of isentropic mixing coefficient

In regions of the stratosphere where large-scale mixing is expected to be caused by the planetary waves, which are quasi-adiabatic, the following parameterization, from (21), is used:

$$\frac{\square\cdot F}{\bar{\sigma}} = -K_{yy}\cos^2\phi\,\frac{\partial}{\partial y}\hat{P}. \qquad (24)$$

The zonal mean wind that enters into the evaluation of the meridional gradient of the zonal mean Ertel's potential vorticity on the right side of (24) has been smoothed through Fourier analysis. This is done to eliminate local small regions where $\partial\hat{P}/\partial y$ changes sign, caused either by noise in the data, or as an indication of local baroclinic and barotropic instability. Charney and Stern (1962) found that a necessary condition for such instability is a sign change of the gradient of Ertel's potential vorticity along isentropic surfaces. Presumably, a consequence of the growth of such unstable waves is to smooth out mean wind gradients so that in time the flow becomes neutral. Since we are not interested in short-time or small-scale processes, the flow is artificially smoothed by discarding the highest few Fourier harmonics in space. Tests show that the derived K_{yy} is not sensitive to the exact level of truncation after the highest few harmonics are discarded. At very high latitude near the poles, the calculation of $\partial\hat{P}/\partial y$ may become problematic because the angular speed $\bar{u}/a\cos\phi$ may be too sensitive to data quality for $\bar{u}$. Here, when the calculated $\partial\hat{P}/\partial y$ changes sign or is too close to zero, K_{yy} is extrapolated from nearby points.

In the easterly wind region (above 40 km in the summer hemisphere), into which planetary waves cannot penetrate, (24) is not expected to hold. Here $\square\cdot F/\bar{\sigma}$ is positive; such easterly deceleration cannot be accomplished by isentropic downgradient transport of Ertel's potential vorticity; and K_{yy} becomes negative if (24) is strictly enforced. Focusing our attention to below 40 km, we show in Fig. 11 the isentropic mixing coefficient, K_{yy}, deduced from (24), multiplied by $\cos^2(\phi)$. (The reader is reminded that our definition of y is $y = a\sin\phi$ instead of $y = a\phi$ in common use. It is probably more appropriate to compare $K_{yy}\cos^2\phi$ using the former definition of y with K_{yy} using the latter definition of y.)

Due to lack of physically based parameterization, earlier 2-D models used a constant mixing coefficient. Kida (1983) and Tung (1984) estimated that the value of constant K_{yy} to be used in a 2-D model should be ~ 3 to 4×10^5 m^2 s^{-1}. While this K_{yy} worked well for most large scale tracers, numerical experiment by Ko et al. (1985) showed that the observed latitudinal structure of nitric acid column density, which has a large latitudinal gradient, cannot be simulated satisfactorily using a constant value of K_{yy}. A small K_{yy} value (less than 3×10^5 m^2 s^{-1}) in the tropics, but larger K_{yy} values (on the order of 10^6 m^2 s^{-1}) in the middle latitudes (see Fig. 12) are probably what is required.

Figure 11 shows our derived K_{yy} field to be latitudinally and seasonally varying. Generally, values of K_{yy} are found to be large ($\sim 10^6$ m^2 s^{-1}) in midlatitudes and smaller ($\sim 10^5$ m^2 s^{-1}) in high latitudes and tropical regions for both hemispheres. Such a bimodal structure is also found to be necessary for a satisfactory simulation of the excess carbon 14 data (Shia et al. 1989).

Above 40 km, the present deduced values for K_{yy} probably cannot be trusted, because the present procedure lumps the gravity wave (vertical) diffusion together with the planetary wave (horizontal) diffusion. When diffusion due to breaking gravity waves in the upper stratosphere and lower mesosphere is taken into account, the K_{yy} values should be lower than what is found here above the stratospheric jet maximum. We also point out that small negative K_{yy} values appear in equatorial regions in April and October. These are found to depend on our procedure for zonal wind extrapolation across the equator under equinox conditions. The extent of negative K_{yy} regions in the troposphere is found to depend on the latent heating and on the particular procedure adopted to enforce mass conservation.

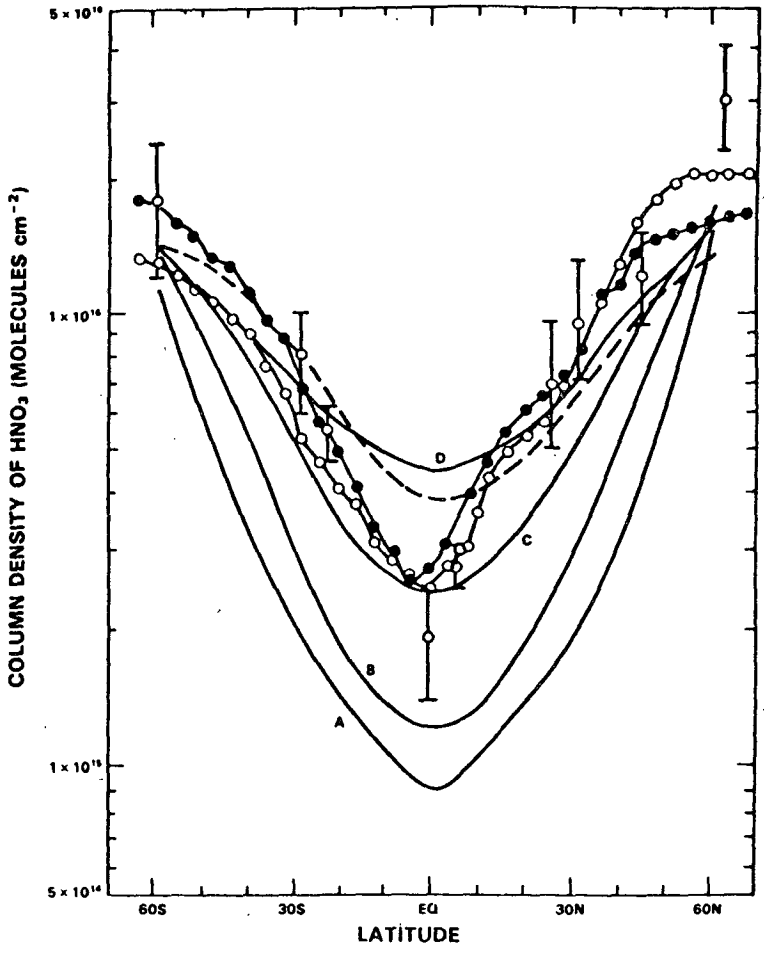

FIG. 12. Comparison of observed (bars for April/May 1980; dash-solid circle curve for May 1979; dash-open circle curve for December, 1978) and simulated nitric acid column density using various constant values of K_{yy} (curve A for $K_{yy} = 0$; curve B for $K_{yy} = 1 \times 10^5$ m^2 s^{-1}; curve C for $K_{yy} = 3 \times 10^5$ m^2 s^{-1}; and curve D for $K_{yy} = 1 \times 10^6$ m^2 s^{-1}), taken from Ko et al. (1985).

Pitari and Visconti (1985), Plumb and Mahlman (1987) have calculated the K_{yy} field using GCM data. Their results being dependent upon the characteristics of the models involved are quite different from ours and from each other in some aspects. In particular, our values of K_{yy} in lower stratosphere tropical region is smaller than theirs, and large values of our K_{yy} are found near the jet maxima, rather than near the zero wind line as in theirs. The occurrence of GCM model K_{yy} maximum near the zero-wind line, which is consistent with weakly nonlinear theories, may be indicative of model wave activity being weaker than in the real atmosphere.

Newman et al. (1988) found that the use of geostrophic winds in the evaluation of quasi-geostrophic potential vorticity flux and gradient yielded large regions of negative K_{yy} values, while the use of nongeostrophic winds showed improvement by reducing the area of negative K_{yy} value regions. They also deduced K_{yy} from momentum balance between quasi-geostrophic potential vorticity flux and residual circulation. Our results, based on nongeostrophic momentum balance between Ertel's potential vorticity gradient and diabatic circulation, appear to improve further. For example, K_{yy} values in January winter stratosphere are positive everywhere.

All our results described so far were deduced from NMC temperature data for 1980. We would like to point out that while the general features are robust, details vary from year to year. In Figs. 13 and 14, we present E–P flux divergence and isentropic mixing coefficient averaged over six years (1979–1984) for the months of January, April, July, and October. In Fig. 15, values of $K_{yy}\cos^2(\phi)$ in lower stratosphere for each individual year are plotted, where K_{yy} values (negative values replaced by zero) from $z_1/H = 1$ to $z_1/H = 4$ are averaged. In this figure, the bimodal structure is clearly illustrated. [The six-year mean value of $(1/\pi)$ $\int_{-\pi/2}^{\pi/2} K_{yy}\cos^2\phi d\phi$ is about 3×10^5 m^2 s^{-1} for the lower stratosphere. Therefore, a constant value of 3

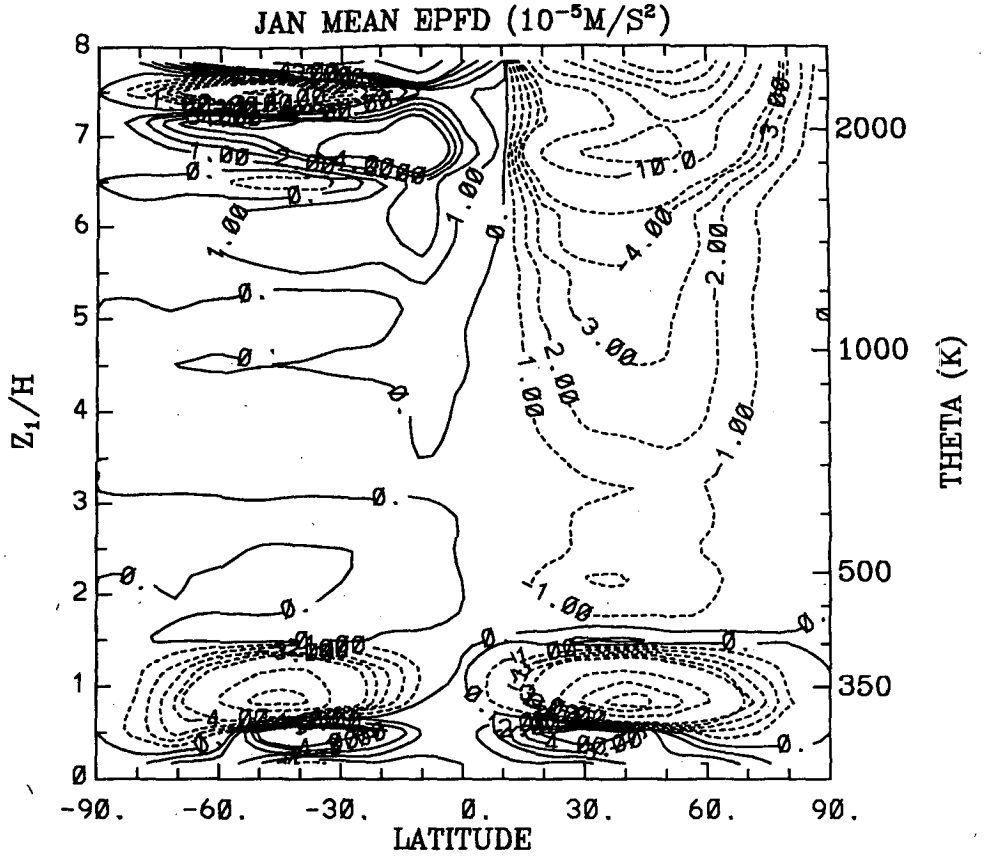

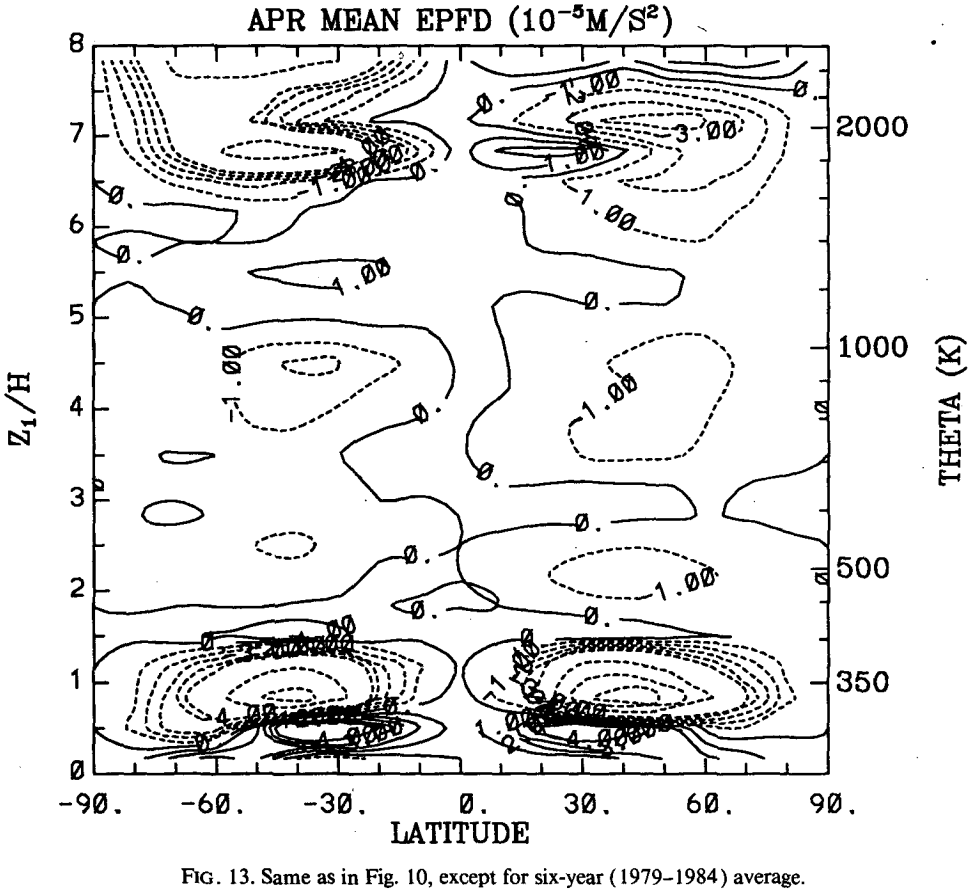

FIG. 13. Same as in Fig. 10, except for six-year (1979–1984) average.

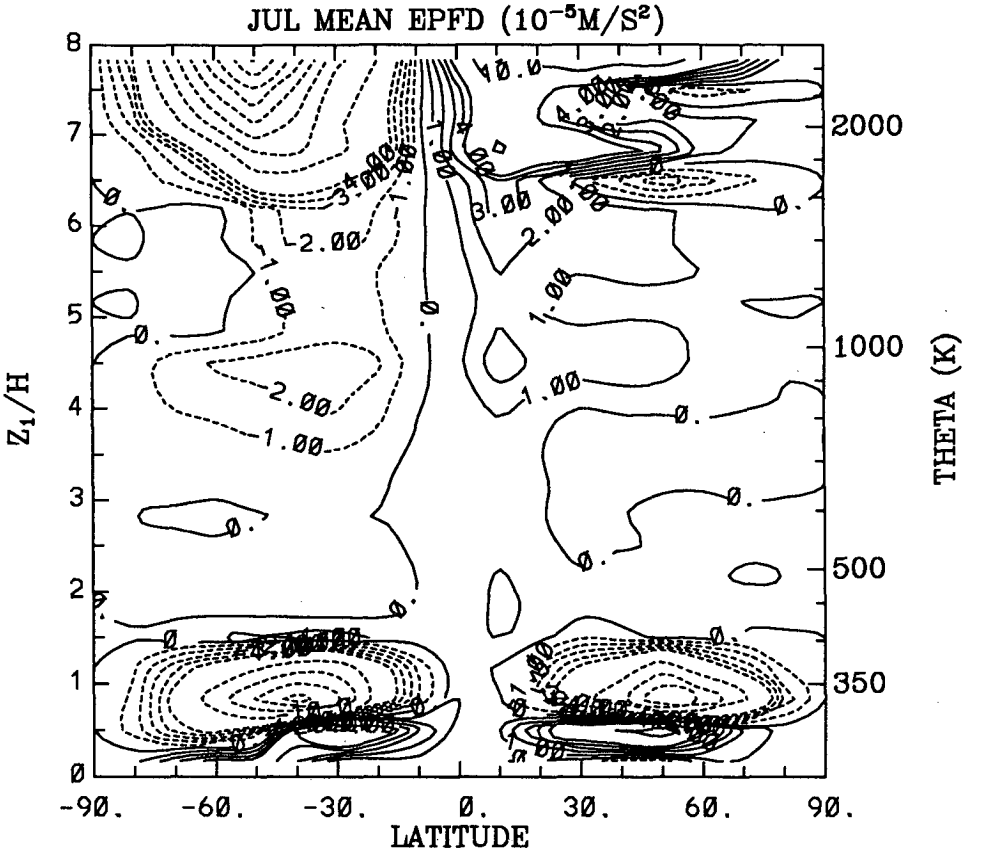

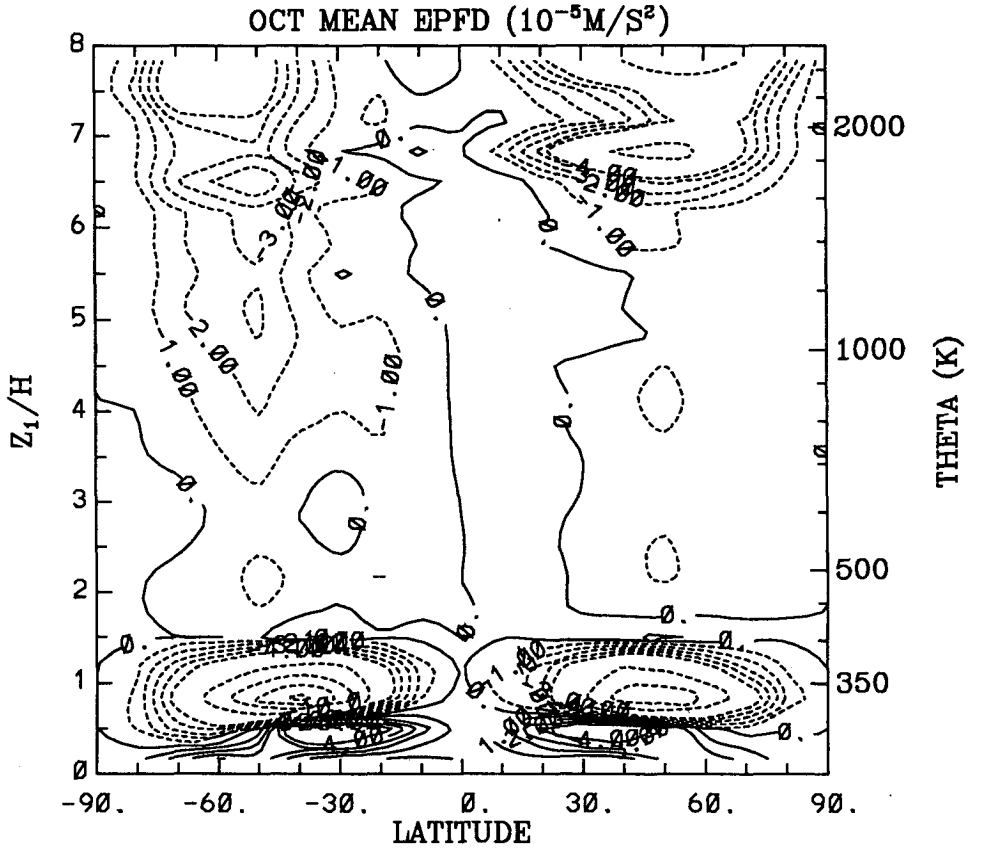

FIG. 13. (*Continued*)

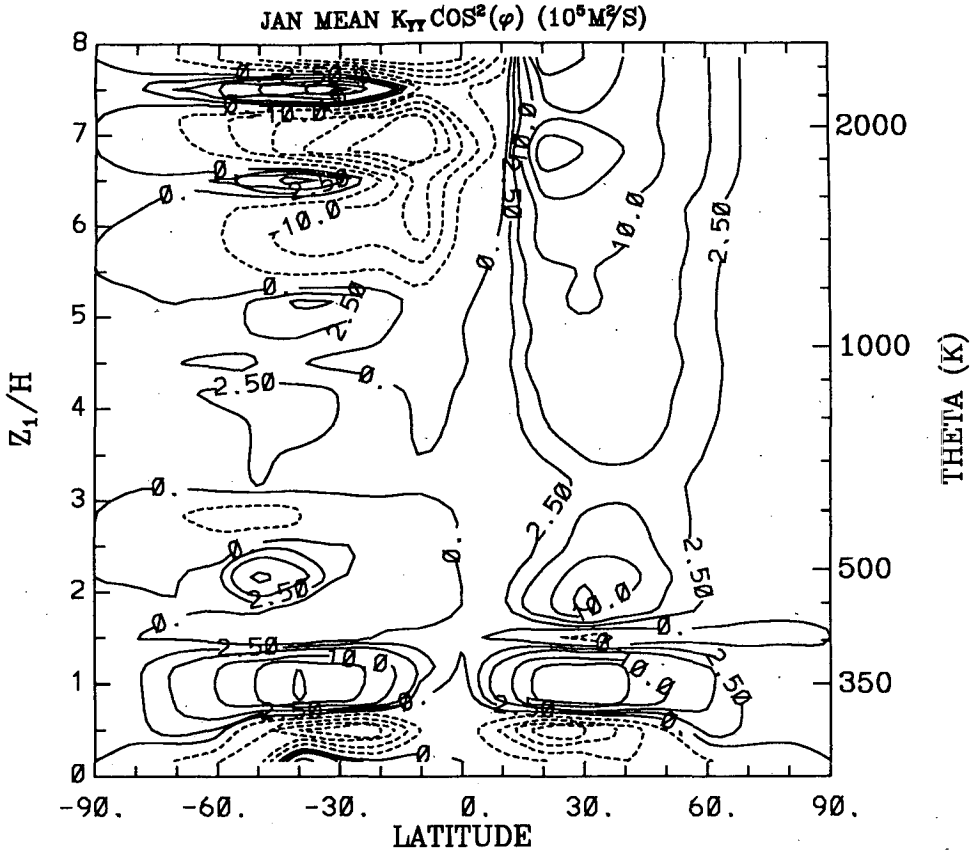

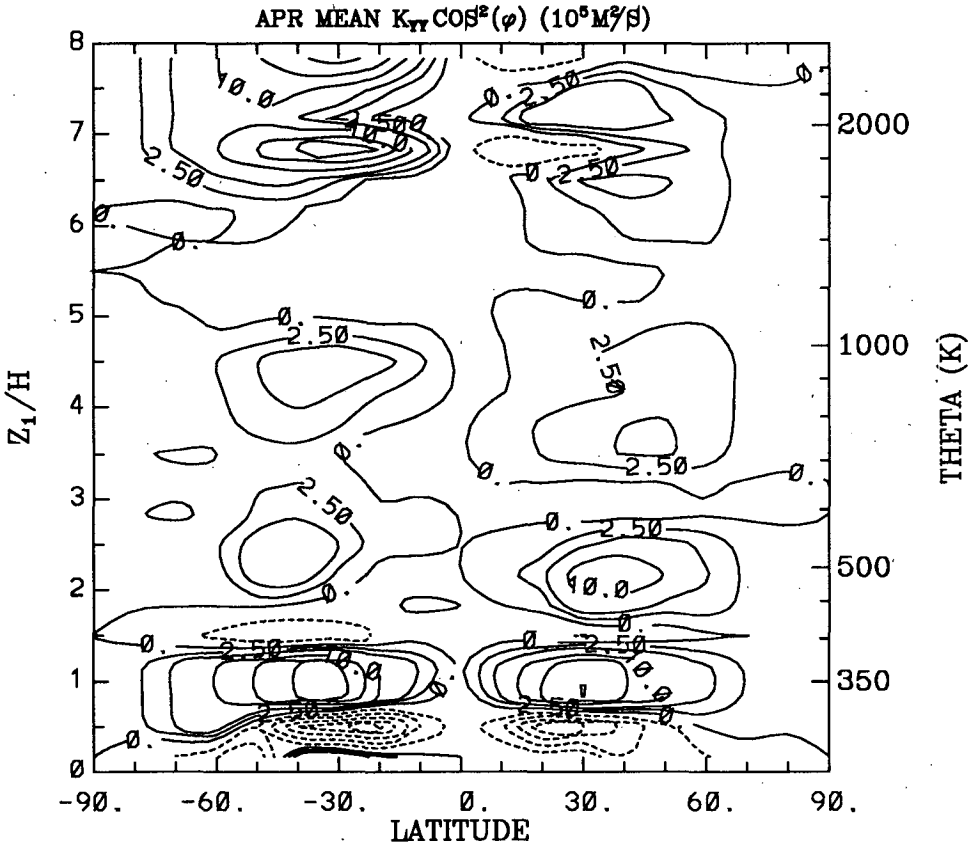

FIG. 14. Same as in Fig. 11, except for six-year (1979–1984) average.

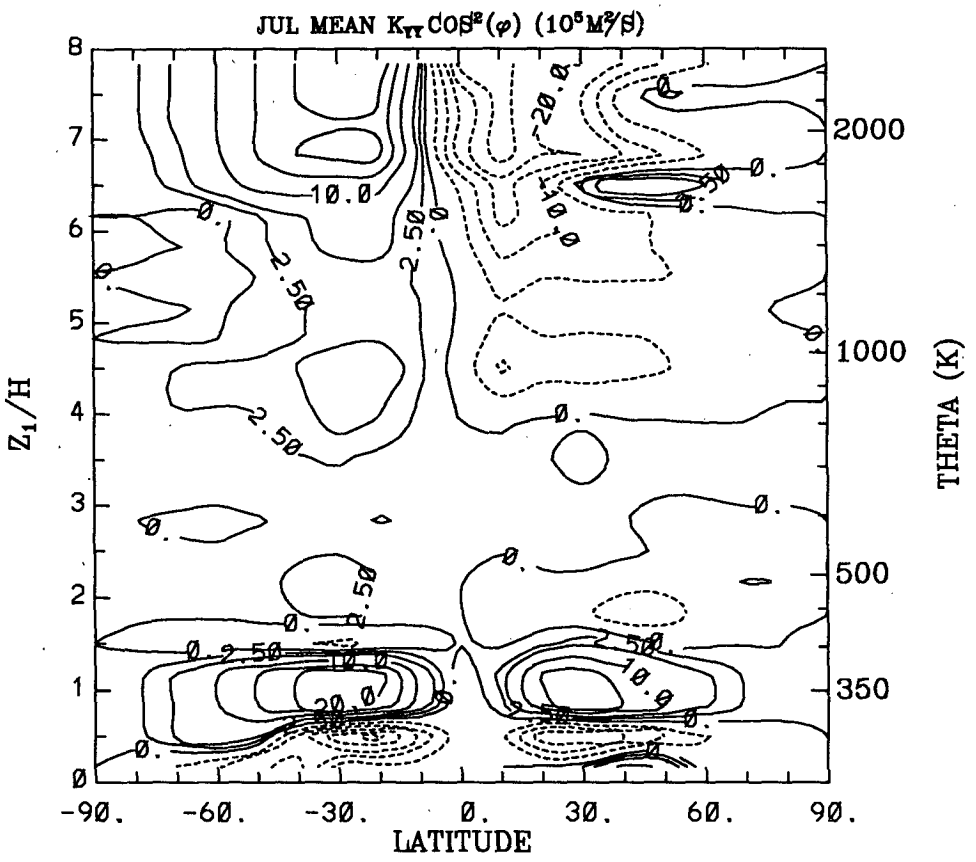

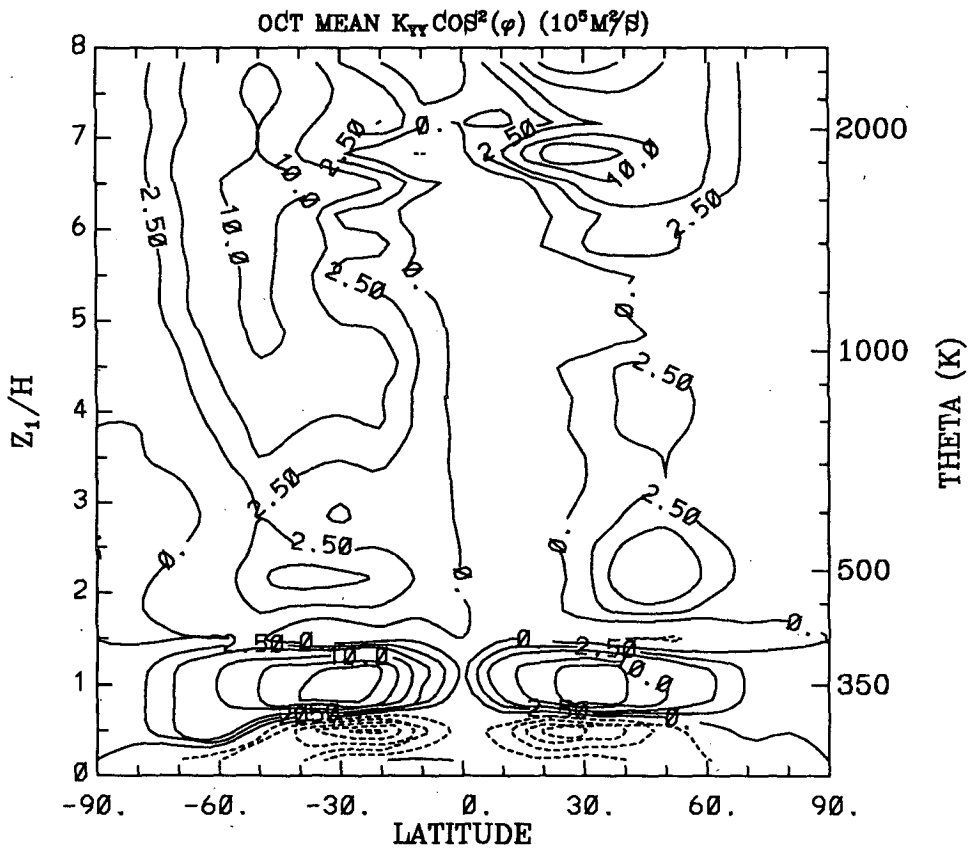

FIG. 14. (*Continued*)

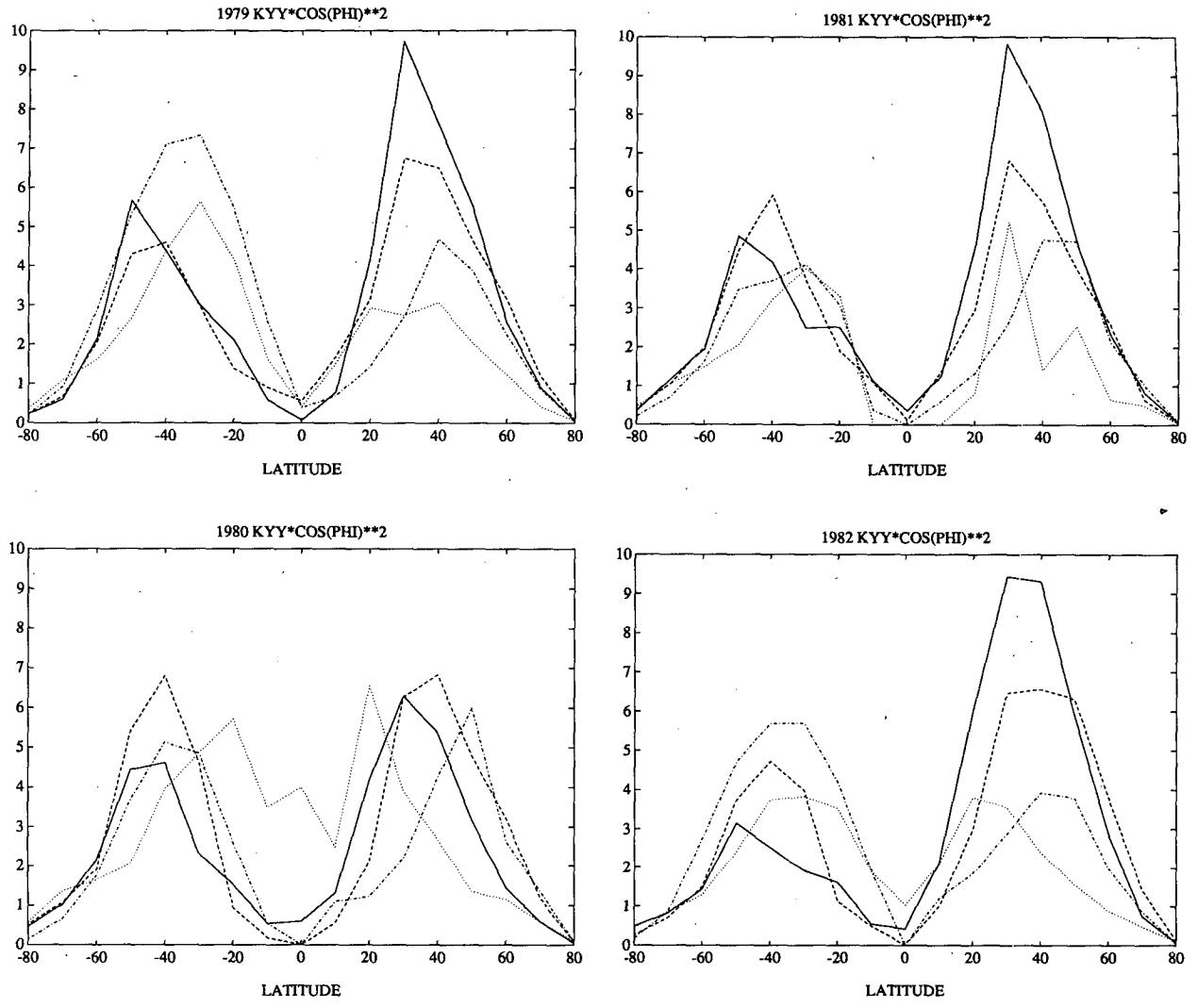

FIG. 15. Calculated isentropic mixing coefficient, $K_{yy}\cos^2(\phi)$, averaged over lower stratosphere ($1 \leq z_1/H \leq 4$) for January (solid), April (dashed), July (dotted) and October (dot-dashed). Unit is 10^5 cm^2 s^{-1}. (a) for 1979; (b) for 1980; (c) for 1981; (d) for 1982; (e) for 1983; (f) for 1984.

$\times 10^5$ m^2 s^{-1} previously used is probably close if only a single constant value is to be used.] One important feature of the K_{yy} field is that in the middle latitude of the lower stratosphere, K_{yy} values are generally larger in the Northern Hemisphere than those in the Southern Hemisphere. The hemispheric asymmetry is almost certainly the manifestation of the fact that the stationary planetary wave activities caused by large-scale continental elevations and land–sea contrasts are stronger in the Northern Hemisphere. Such features of K_{yy}, together with a consistent diabatic circulation, made it possible for us to simulate many features of the observed ozone distribution (Tung and Yang 1988).

6. Advective and diffusive transports

In zonally averaged models of tracer transport, two types of transport processes exist: advective and diffusive transports. The separation of these two processes is most distinct when the zonal average is taken on isentropic surfaces (see Tung 1982). In this coordinate system, the advective transport is predominantly effected through the Eulerian zonal mean meridional circulation, which is also the same as the diabatic circulation. And diffusion acts predominantly along the isentropes over the bulk of the stratosphere.

For a tracer whose mass mixing ratio is χ and whose chemical sources and sinks are denoted by S, the transport equation is, in three dimensions,

$$\frac{d\chi}{dt} = S. \tag{25}$$

The zonal average (along surfaces of constant potential temperature) is approximately (see Tung 1982, 1984, 1987)

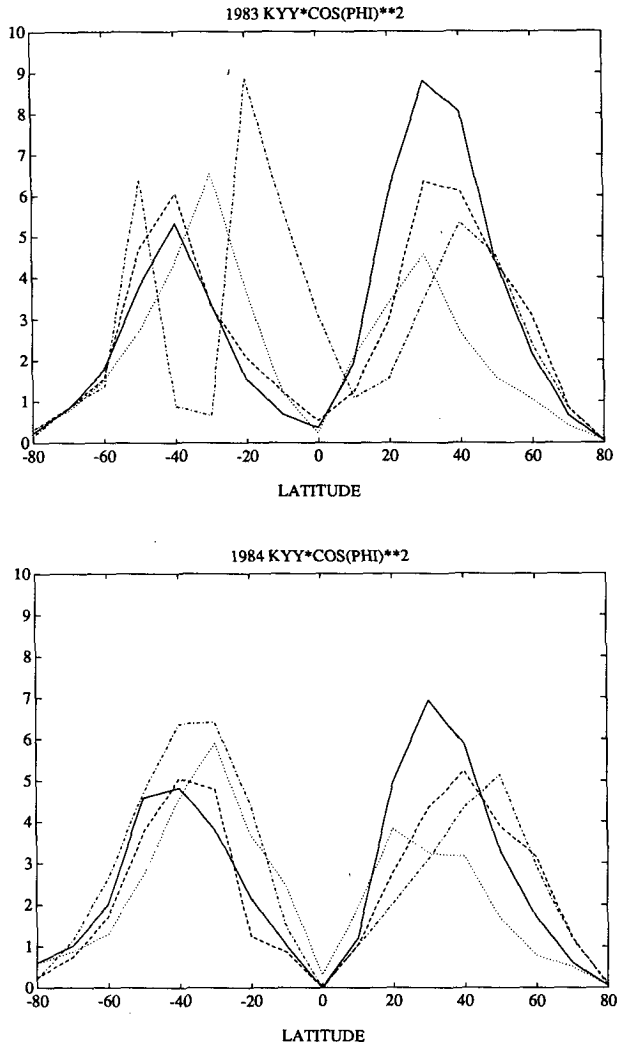

FIG. 15. (*Continued*)

$$\bar{\sigma}\frac{\partial \bar{\chi}}{\partial t} + \bar{V}\frac{\partial \bar{\chi}}{\partial y} + \bar{W}\frac{\partial \bar{\chi}}{\partial z_1} = \frac{\partial}{\partial y}\bar{\sigma}K_{yy}\cos^2\phi\frac{\partial \bar{\chi}}{\partial y} + \bar{\sigma}\bar{S}. \tag{26}$$

In Eq. (26), "chemical eddy" terms, which contribute to diffusion transport, are neglected. Tung (1984) showed that the chemical eddy modification to the diffusion term can be neglected for chemical tracers whose lifetime is longer than a couple of weeks. In regions with significant breaking gravity waves, a $K_{z_1z_1}$-type of cross-isentropic diffusion should also be added to (26). Equation (26) is expected to hold approximately over the bulk of stratosphere below 40 km.

The 2-D form of tracer transport equation (26) shows that the dominant forms of transport are advection by the zonal meridional circulation ($\bar{V}$, $\bar{W}$) and diffusion along isentropes with isentropic mixing coefficient K_{yy}. We have described in this paper how both can be determined self-consistently from the same observed mean temperature field $\bar{T}$. A 2-D model based on this type of self-consistently determined transport parameters is termed the "third generation" 2-D model by Tung (1987), as to be distinguished from the "second generation" 2-D model, where ($\bar{V}$, $\bar{W}$) and K_{yy} are separately, and perhaps inconsistently, specified (see Ko et al. 1985). The "first generation" of 2-D models used Eulerian mean meridional circulation in pressure coordinates as the advective transport and empirically determined diffusion along a hypothetical "mixing path" (see Reed and German 1965). The present work indicates that a physically based, easily implementable procedure exists that allows both the advective and diffusive transports to be self-consistently calculated for use in a "third generation" 2-D model.

We have constructed such a coupled model and found it more successful in simulating the observed distributions of many photochemical tracer species. The result are described in Yang et al. (1989). Of many chemical species simulated simultaneously with the coupled model, one of them is nitric acid, which has been mentioned in section 5 to be a species that can be used to constrain the value and structure of K_{yy}, as noted previously by Ko et al. (1985). Figure 16 shows the column nitric acid simulated using the variable K_{yy} reported here (along with the advective transport consistent with it; negative K_{yy} values are replaced by zero). The comparison for May (which does not have a polar

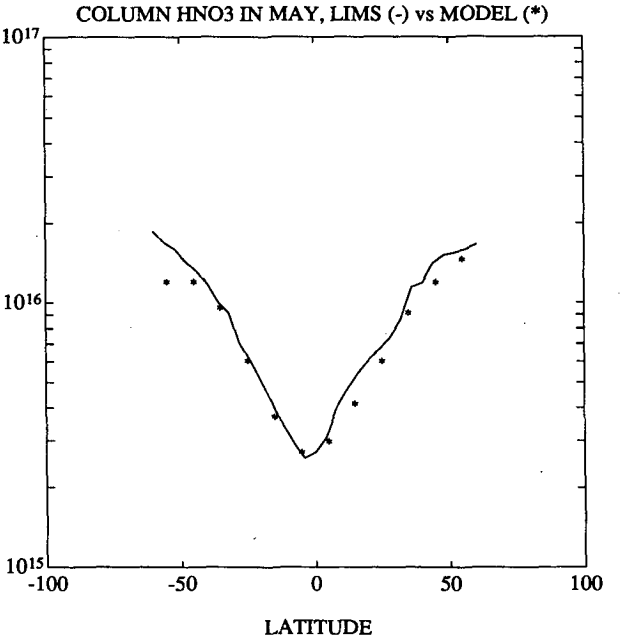

FIG. 16. Comparison of observed (for May 1979, as shown in Fig. 12) and model simulated nitric acid column density for May 1980 using K_{yy} values deduced in this paper.

night) shows excellent agreement, including the V-shaped profile that was found observationally and was difficult to reproduce by models with constant K_{yy}'s.

7. Conclusion

We have performed a diagnostic study of the Eliassen–Palm flux divergence based on the nongeostrophic theory of zonally averaged circulation of Tung (1986). Regions of positive divergence of Eliassen–Palm flux that were found to be present by other authors using quasi-geostrophic approximation in high latitude winter stratosphere largely disappear under the present nongeostrophic formulation. The long-term (monthly) averaged effect of eddies is generally to decelerate the mean flow in the entire stratosphere for all seasons, so that the jets are weaker than they would have been in the absence of eddies. Further improvements can be obtained if a dataset of the zonal winds is available. In this study, $\bar{u}$ is determined from $\bar{T}$ using the gradient wind relationship, which breaks down near the equator.

Also, we have given a physically based procedure and diagnostically calculated the isentropic mixing coefficient field, which is consistent with the advective transport field. Nongeostrophic momentum balance between Ertel's potential vorticity gradient and diabatic circulation yields positive K_{yy} values in most of the places, except for regions where our parameterization breaks down (e.g., lower troposphere and upper summer stratosphere) or where our procedure suffers large uncertainties (e.g., uncertainties in equatorial winds). Our results show that K_{yy} varies considerably in space and time. In particular, the values in middle latitudes are higher than those in tropical and polar regions.

The validity and usefulness of our parameterization of K_{yy} can be tested using a zonally averaged model. In Tung and Yang (1988), the same procedure was applied to a 2-D model with simplified radiative transfer calculation and parameterized chemistry, and many observed climatological features of global ozone distribution was simulated. In Yang et al. (1989), we describe a coupled 2-D model with the dynamics discussed above, advanced radiative transfer codes and detailed chemistry. The simulated distribution of many stratospheric species have been improved over earlier model results using specified constant K_{yy}. We showed here in particular the simulation of nitric acid had been more satisfactory over previous model calculations.

Acknowledgments. We are grateful to Drs. David Wu, Eric Nash and Paul Newman for making NMC data available to us in a convenient form. We would like to thank Dr. Jerry Mahlman and another anonymous reviewer for their helpful comments. The research is sponsored by NASA under Grants NAGW-910 and NAGW-1605.

REFERENCES

Andrews, D. G., 1983: A finite-amplitude Eliassen–Palm theorem in isentropic coordinates. *J. Atmos. Sci.*, **40,** 1877–1883.

——, and M. E. McIntyre, 1978a: Generalized Eliassen–Palm and Charney–Drazin theorems for waves on axisymmetric mean flows in compressible atmosphere. *J. Atmos. Sci.*, **35,** 2031–2048.

——, and ——, 1978b: On wave action and its relatives. *J. Fluid Mech.*, **89,** 647–664.

——, J. D. Mahlman and R. W. Sinclair, 1983: Eliassen–Palm diagnostics of wave, mean-flow interaction in the GFDL "SKYHI" general circulation model. *J. Atmos. Sci.*, **40,** 2768–2784.

——, J. R. Holton and C. B. Leovy, 1987: *Middle Atmosphere Dynamics,* Academic Press, 489 pp.

Bretherton, F. P., 1966: Critical layer instability in baroclinic flows. *Quart. J. Roy Meteor. Soc.*, **92,** 325–334.

Callis, L. B., R. E. Boughner and J. D. Lambeth, 1987: The stratosphere: climatologies of the radiative heating and cooling rates and the diabatically diagnosed net circulation fields. *J. Geophys. Res.*, **90,** 5585–5607.

Charney, J. G., and M. E. Stern, 1962: On the stability of internal baroclinic jets in a rotating atmosphere. *J. Atmos. Sci.*, **19,** 159–172.

Clough, S. A., N. S. Graham and A. O'Neill, 1985: Potential vorticity in the stratosphere derived using data from satellite. *Quart. J. Roy. Meteor. Soc.*, **111,** 335–358.

Danielson, E. F., 1981: An objective method for determining the generalized transport tensor for two-dimensional Eulerian models. *J. Atmos. Sci.*, **38,** 1319–1339.

Dickinson, R. E., 1969: Theory of planetary waves, zonal-mean flow interaction. *J. Atmos. Sci.*, **26,** 73–81.

Dopplick, T. G., 1972: Radiative heating of the global atmosphere. *J. Atmos. Sci.*, **29,** 1278–1294.

——, 1979: Radiative heating of the global atmosphere: Corrigendum. *J. Atmos. Sci.*, **36,** 1812–1817.

Dunkerton, T., 1978: On the mean meridional motions of the stratosphere and mesosphere. *J. Atmos. Sci.*, **35,** 2325–2333.

Edmon, H. J., Jr., B. J. Hoskins and M. E. McIntyre, 1980: Eliassen–Palm cross sections for the troposphere. *J. Atmos. Sci.*, **37,** 2600–2616. (Corrigendum, *J. Atmos. Sci.*, **38,** 1115, 1981.)

Fels, S. B., J. D. Mahlman, M. D. Schwarzkopf and R. W. Sinclair, 1980: Stratospheric sensitivity to perturbations in ozone and carbon dioxide: Radiative and dynamical response. *J. Atmos. Sci.*, **37,** 2265–2297.

Fritts, D. C., T. Tsuda, T. E. VanZandt, S. A. Smith, T. Sato, S. Fukao and S. Kato, 1989: Studies of velocity fluctuations in the upper atmosphere using the MU radar. Part II: Momentum fluxes and energy density. *J. Atmos. Sci.*, in press.

Geller, M. A., M. F. Wu and M. E. Gelman, 1983: Troposphere–stratosphere (surface–55 km) monthly winter general circulation statistics for the Northern Hemisphere—four year average. *J. Atmos. Sci.*, **40,** 1334–1352.

——, —— and ——, 1984: Troposphere–stratosphere (surface–55 km) monthly winter general circulation statistics for the Northern Hemisphere—interannual variations. *J. Atmos. Sci.*, **41,** 1726–1744.

——, and ——, 1987: Troposphere–stratosphere general circulation statistics. *Transport Processes in the Middle Atmosphere,* G. Visconti and R. R. Garcia, Eds., D. Reidel.

Green, J. S. A., 1970: Transfer properties of the large-scale eddies and the general circulation of the atmosphere. *Quart. J. Roy. Meteor. Soc.*, **96,** 157–185.

Hartmann, D. L., C. R. Mechoso and K. Yamazaki, 1984: Observation of wave-mean flow interactions in the Southern Hemisphere. *J. Atmos. Sci.*, **41,** 351–362.

Haynes, P. H., and M. E. McIntyre, 1987: On the evolution of vorticity and potential vorticity in the presence of diabatic heating and frictional or other forces. *J. Atmos. Sci.*, **44,** 828–841.

Holton, J. R., 1980: Wave propagation and transport in the middle atmosphere. *Phil. Trans. Roy. Soc. London,* **A296,** 73–85.

——, 1981: An advective model for two-dimensional transport of stratospheric trace species. *J. Geophys. Res.,* **86,** 11989–11994.

——, 1986: Meridional distribution of stratospheric trace constituents. *J. Atmos. Sci.,* **43,** 1238–1242.

Kida, H., 1983: General circulation of air parcels and transport characteristics derived from a hemisphere GCM. Part 2: Very long-term motions of air parcels in the troposphere and stratosphere. *J. Meteor. Soc. Japan,* **61,** 510–523.

Kiehl, J. T., and S. Solomon, 1986: On the radiative balance of the stratosphere. *J. Atmos. Sci.,* **43,** 1525–1534.

Ko, M. K. W., K. K. Tung, D. K. Weisenstein and N. D. Sze, 1985: A zonal mean model of stratospheric tracer transport in isentropic coordinates: Numerical simulation for nitrous oxide and nitric acid. *J. Geophys. Res.,* **90,** 2313–2329.

Lettau, H., 1951: Diffusion in the upper atmosphere. *Compendium of Meteorology,* T. F. Malone, Ed., Amer. Meteor. Soc., 320–333.

Lindzen, R. S., 1981: Turbulence and stress owing to gravity wave and tidal breakdown. *J. Geophys. Res.,* **86,** 9707–9714.

Lorenz, E. N., 1955: Available potential energy and the maintenance of the general circulation. *Tellus,* **7,** 157–167.

Mahlman, J. D., 1985: Mechanistic interpretation of stratospheric tracer transport. *Adv. Geophys.,* **28A,** 301–323.

——, and L. J. Umscheid, 1984: Dynamics of the middle atmosphere: Successes and problems of the GFDL "SKYHI" general circulation model. *Dynamics of the Middle Atmosphere,* J. R. Holton and T. Matsuno, Eds., Terra Scientific, 501–525.

——, D. G. Andrews, D. L. Hartmann, T. Matsuno and R. G. Murgatroyd, 1984: Transport of trace constituents in the stratosphere. *Dynamics of the Middle Atmosphere,* J. R. Holton and T. Matsuno, Eds., Terra Scientific, 387–416.

Matsuno, T., 1980: Lagrangian motion of air parcels in the stratosphere in the presence of planetary waves. *Pure Appl. Geophys.,* **118,** 189–216.

McPeters, R. D., D. F. Heath and P. K. Bhartia, 1984: Average ozone profiles for 1979 from the NIMBUS 7 SBUV instrument. *J. Geophys. Res.,* **89,** 5199–5214.

Murgatroyd, R. J., and F. Singleton, 1961: Possible meridional circulations in the stratosphere and mesosphere. *Quart. J. Roy. Meteor. Soc.,* **87,** 125–135.

Newman, P. A., M. R. Schoeberl and R. A. Plumb, 1986: Horizontal mixing coefficients for two-dimensional chemical models calculated from National Meteorological Center data. *J. Geophys. Res.,* **91,** 7919–7924.

——, ——, —— and J. E. Rosenfield, 1988: Mixing rates calculated from potential vorticity. *J. Geophys. Res.,* **93,** 5221–5240.

Olaguer, E., and H. Yang, 1989: A fast quasi-narrow band radiative transfer algorithm for use in stratospheric models. *J. Geophys. Res.,* submitted.

Palmer, T. N., and C.-P. F. Hsu, 1983: Stratospheric sudden cooling and the role of nonlinear wave interactions in preconditioning the circumpolar flow. *J. Atmos. Sci.,* **40,** 909–928.

Patari, G., and G. Visconti, 1985: Two-dimensional tracer transport: Derivation of residual mean circulation and eddy transport tensor from a 3-D model data set. *J. Geophys. Res.,* **90,** 8019–8032.

Pawson, S., and R. S. Harwood, 1988: Monthly-mean diabatic circulations in the stratosphere, *Quart. J. Roy. Meteor. Soc.,*

Phillips, N. A., 1957: A coordinate system having some special advantages for numerical forecasting. *J. Meteor.,* **14,** 184–185.

Plumb, R. A., 1979: Eddy fluxes of conserved quantities by small-amplitude waves. *J. Atmos. Sci.,* **36,** 1699–1704.

——, and J. D. Mahlman, 1987: The zonally averaged transport characteristics of the GFDL general circulation/transport model. *J. Atmos. Sci.,* **44,** 298–327.

Reed, R. J., and K. E. German, 1965: A contribution to the problem of stratospheric diffusion by large-scale mixing. *Mon. Wea. Rev.,* **93,** 313–321.

Robinson, W. A., 1986: On the application of the quasi-geostrophic Eliassen–Palm flux to the analysis of stratospheric data. *J. Atmos. Sci.,* **43,** 1017–1023.

Rosenfield, J. E., M. R. Schoeberl and M. A. Geller, 1987: A computation of the stratosphere diabatic circulation using an accurate radiative transfer model. *J. Atmos. Sci.,* **44,** 859–876.

Shia, R. L., Y. L. Yung, M. Allen, R. W. Zurek and D. Crisp, 1989: Sensitivity study of advection and diffusion coefficients in a two-dimensional stratospheric model using excess carbon 14 data. Submitted to *J. Geophys. Res.*

Shine, K., 1989: Sources and sinks of zonal momentum in the middle atmosphere diagnosed using the diabatic circulation. *Quart. J. Roy. Meteor. Soc.,* **115,** 265–292.

Taylor, G. I., 1915: Eddy motion in the atmosphere. *Phil. Trans. Roy. Soc. London.* **A215,** 1–26.

Tung, K. K., 1982: On the two-dimensional transport of stratospheric trace gases in isentropic coordinates. *J. Atmos. Sci.,* **39,** 2330–2355.

——, 1984: Modeling of tracer transport in the middle atmosphere. *Dynamics of the Middle Atmosphere,* J. R. Holton and T. Matsuno, Eds., Terra Scientific Publishing, 412–444.

——, 1986: Nongeostrophic theory of zonally averaged circulation. Part I: formulation. *J. Atmos. Sci.,* **43,** 2600–2618.

——, 1987: A coupled model of zonally averaged dynamics, radiation and chemistry. *Transport Processes in the Middle Atmosphere,* G. Visconti and R. R. Garcia, Eds., D. Reidel.

——, and H. Yang, 1988: Dynamical component of seasonal and year-to-year changes in Antarctic and global ozone. *J. Geophys. Res.,* **93,** 12537–12559.

World Meteorological Organization, 1986: Atmospheric Ozone 1985: Assessment of our understanding of processes controlling its present distribution and change, Geneva, Switzerland. *WMO Rep. 16,* Global Ozone Res. and Monit. Proj.

Yang, H., E. Olaguer and K. K. Tung, 1989: Simulation of the present-day chemical composition of the stratosphere using a coupled 2-D model in isentropic coordinates. *J. Atmos. Sci.,* submitted.